Theor Chim Acta (1991) 78: 327–363

Theoretica Chimica Acta

The ring opening of cyclopropylidene to allene and the isomerization of allene: *ab initio* interpretation of the electronic rearrangements in terms of quasi-atomic orbitals

S. Xantheas*, P. Valtazanos, and K. Ruedenberg
Ames Laboratory, USDOE**, and Department of Chemistry, Iowa State University, Ames, IA 50011, USA

Received August 30, 1990/Accepted September 5, 1990

Summary. A full optimized reaction space (FORS) remains invariant under arbitrary orthogonal transformations among its configuration-generating molecular orbitals. Localization of the latter for a FORS wavefunction yields molecular orbitals with *quasi-atomic* character which can be interpreted as *molecule-adapted minimal-basis-set atomic orbitals*. In terms of these quasi-atomic FORS MOs, the configuration mixing in the FORS wavefunction, the representation of the density matrix, and the expansions of the natural orbitals provide information about the interactions that are responsible for the molecular energy changes. A basis-set-independent population analysis can be formulated which accomplishes the objectives of Mulliken's population analysis without the drawbacks stemming from the basis-set dependence of the latter. Through application of these procedures, explanations can be found for various features of the potential energy surface governing the ring opening of cyclopropylidene and the isomerization of allene.

Key words: Cyclopropylidene to allene – Orbital interpretation of electronic rearrangements – Potential energy surface

1. Introduction

Upon examining the energy changes that are exhibited by a potential energy surface with the complexity of that found for the cyclopropylidene ground-state ring opening [1, 2] chemists can be expected to ask whether *ab-initio* theory can also produce insightful *explanations* for the computed energy changes. In view of the advances made over the past decade in quantum-chemical calculations it stands to reason that one would hope for equally rigorous quantifications regarding the interpretation of such calculations in temrs of chemical and physical concepts.

* *Present address:* Molecular Sciences Research Center, Pacific Northwest Laboratory, Richland, WA 99352, USA

** Operated for the U.S. Department of Energy by Iowa State University under contract No. 7405-ENG-82. This work was supported by the Office of Basic Energy Sciences

A fundamental tenet of intuitive chemical thinking is the interpretation of molecules in terms of *interactions between atoms*. Such an interpretation does not emerge trivially from *ab initio* quantum chemistry because, in principle, all electrons in a molecule must be treated on an equal footing and molecular wavefunctions must be antisymmetrized with respect to all electronic coordinates. Moreover, decompositions in terms of atomic contributions present particular difficulties in the simplest and most widely used *ab-initio* method, namely the conventional Hartree–Fock self-consisted-field model. This is because, even in their most localized forms, self-consistent-field *bonding* orbitals necessarily cover several atoms. Any decomposition of such orbitals in terms of atomic contributions requires a split of individual bonding MOs into parts which are assigned to different atoms. Such segmentations (as, for example, formalized by Mulliken's population analysis) are fundamentally arbitrary, they tend to be basis-set dependent and, for calculations with extended basis sets, they often loose their meaning. Since multiconfigurational calculations are inherently more complex than the SCF approach, there may exist a perception that the problem of interpreting molecules in terms of atoms becomes even more difficult when proceeding from the SCF approximation to more sophisticated descriptions. In any event, there do not yet exist well-established quantitative *ab-initio* procedures for the interpretation of bonding interactions between atoms in a molecular system, in particular when the latter is far from its equilibrium positions.

Through the present investigation we hope to show that the situation is much more favorable when one considers molecular wavefunctions obtained within the FORS framework even though the latter is considerably more sophisticated than the self-consistent-field (SCF) model. It is a multiconfiguration-self-consistent-field (MCSCF) approach that includes the major fraction of that part of the electron correlation energy which changes in the course of a reaction. Nonetheless, the FORS model provides, without arbitrary additional assumptions, an effective vehicle for the analysis of molecular systems in terms of atomic subsystems. It leads in a natural manner to definitions of deformed atoms in molecules and of interactions between them.

We shall use this approach here to gain insight into the electronic rearrangements that occur during the cyclopropylidene ring opening. In particular, we shall examine the ring-opening barrier, the allene isomerization barrier and the cogwheel-type free synchronized rotations of the CH_2 groups. The understanding obtained in this manner for this reaction is found to fit in with the spirit of physical organic chemistry. This result suggests that the developed analysis, based on FORS wavefunctions, can yield *ab-initio* interpretations which may furnish the foundation for a closer integration of *ab-initio* calculations and chemical intuition.

2. Methods of analysis

2.1. Localized FORS MOs as molecule-adapted deformed minimal-basis-set atomic orbitals: quasi-atomic orbitals

The nature of FORS wavefunctions is described in Sect. 2.1 of the first paper in this series [1]. It is described in more detail in several previous publications [3]. Two facts are essential in the present context:

(i) FORS wavefunctions are obtained by an MCSCF procedure in a *full configuration space*, i.e., they are expanded in terms of *all* configurations that can be generated from a given set of "reactive" or "active" orbitals;

(ii) The *number* of these *configuration-generating* orbitals is equal to the *number* of conceptual minimal-basis atomic orbitals that are involved in the reaction under study.

The interpretative procedure to be described here takes advantage of the circumstance that a *full configuration space remains invariant when the molecular orbitals which generate the configurational basis are subjected to orthogonal transformations*. Such orbital transformations do yield *new configurational bases*, but these *span the same configuration space*. The *same* (optimal) wavefunction can therefore be expressed as a superposition of many different types of configurations.

Several sets of FORS molecular orbitals prove useful for the case at hand. They will be called:

(i) quasi-atomic FORS MOs,
(ii) natural FORS MOs,
(iii) chemically localized FORS MOs.

The various orbital bases, and the associated configurational bases generate different (but equivalent) descriptions of the arrangements of the electrons in a molecule and, thereby, illustrate different aspects of one and the same electronic distribution. They furnish complementary insights which can be combined to yield a balanced interpretation of the electronic structure.

It is expedient to begin with the quasi-atomic FORS orbitals. This molecular orbital set results from localizing the configuration-generating FORS MOs as much as possible. It has been demonstrated in detail in a series of previous publications [3], and it will be seen again here, that such maximally localized FORS MOs have the character of *molecule-adapted deformed minimal-basis-set atomic orbitals*. They effect an *intrinsic partitioning of the electron population according to atoms* and we therefore call them *quasi-atomic MOs*.

In the case at hand we have a wavefunction with a *nine-orbital SCF-type core* and a *full reactive space generated by four electrons in four reactive orbitals*. In such a case the core orbitals and the reactive orbitals must be localized separately. The localization of the core orbitals yields three inner shell orbitals on the three carbons, two carbon-carbon sigma bonds (for C_0C_1 and C_0C_2) and four carbon-hydrogen sigma bonds. The localization of the four reactive FORS MOs, on the other hand, yields quasi-atomic molecular orbitals $|0\rangle$, $|0'\rangle$, $|1\rangle$, $|2\rangle$ which, as we shall see, look very much like the *reactive atomic valence orbitals* that are qualitatively sketched in Fig. 1 for the reactant (cyclopropylidene), the product (linear staggered allene), and the allene isomerization transition state (bent planar allene).

2.2. Density and population analysis of a FORS wavefunction

Meaningful insights into the electronic structure are obtained by examining the *electron density* kernel ϱ of the FORS wavefunction. The expansion of ϱ in terms of the aforementioned quasi-atomic localized FORS MOs has the form

$$\varrho = 2\sum_{\nu} |\nu\rangle\langle\nu| + \sum_{i,j} p_{ij} |i\rangle\langle j|, \tag{2.1}$$

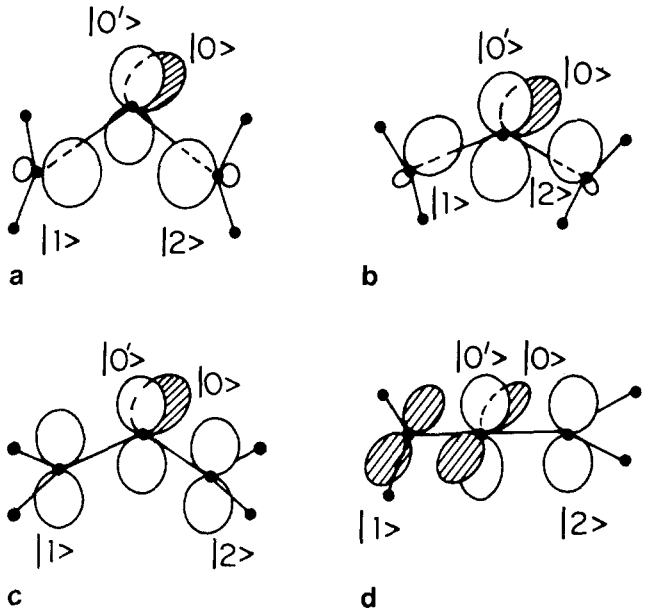

Fig. 1a–d. Qualitative sketch of quasi-atomic FORS MOs. **a** Cyclopropylidene; **b** transition state; **c** allene isomerization transition state; **d** allene

where the index v runs over the nine localized core MOs and the indices i, j run over the four localized reactive MOs, i.e., the quasi-atomic orbitals $|0\rangle, |0'\rangle, |1\rangle, |2\rangle$.

Because of the orbital orthogonality the diagonal elements of the density matrix $\boldsymbol{p}$ lie between 1 and 2 and they are the *rigorous occupation numbers* of the localized FORS MOs. Since the latter are quasi-atomic orbitals, the p_{ii} yield therefore directly an *unambiguous population analysis in terms of the orthogonalized deformed atoms in the molecule.*

Furthermore, since the bonding and antibonding contributions to the molecular energy can be shown to arise predominantly from *interference energy terms* of the type $p_{ij}\langle i|h|j\rangle$, the off-diagonal density matrix elements p_{ij} have the significance of *bond orders* which locate bonding, nonbonding and antibonding effects between the different quasi-atomic orbitals, depending upon appropriate values of the resonance integrals $\langle i|h|j\rangle$. From the example of a doubly occupied diatomic homonuclear molecular orbital, which is expressed in terms of two orthogonalized atomic orbitals as $\phi = (A + B)/\sqrt{2}$, it can be seen that the maximum absolute value which this type of bond order can assume is unity.

Further insight into the nature of the density matrix p_{ij} is obtained by bringing it into diagonal form. This transformation yields the natural MOs [4]. If the orthogonal matrix $\boldsymbol{T}$ diagonalizes the matrix $\boldsymbol{p}$, then we have

$$(\boldsymbol{T}^{+}\boldsymbol{p}\boldsymbol{T})_{nm} = N_n \delta_{nm}, \tag{2.2}$$

whence

$$p_{ij} = \sum_n N_n T_{in} T_{jn}. \tag{2.3}$$

With the help of Eq. (2.3) the density is easily expressed as

$$\varrho = 2\sum_{\nu} |\nu\rangle\langle\nu| + \sum_{n} N_n |\psi_n\rangle\langle\psi_n|, \tag{2.4}$$

where the

$$\psi_n = \sum_{i} \chi_i T_{in} \tag{2.5}$$

are the *natural FORS MOs expressed in terms of the quasi-atomic FORS MOs* χ_i. *The eigenvalues* N_n *are the occupation numbers of the natural FORS MOs* ψ_n.

The quasi-atomic and the natural representations of the density can be combined into a decomposition scheme which is conceptually close in spirit to Mulliken's population analysis [5]. It is obtained by defining the intermediate *population contributions*

$$p_{ii}^{n} = N_n T_{in} T_{in}, \tag{2.6}$$

which can be summed in two ways, namely:

$$\sum_{n} p_{ii}^{n} = p_{ii} \quad \text{and} \quad \sum_{i} p_{ii}^{n} = N_n. \tag{2.7}$$

Similarly, the bond orders can be decomposed into natural orbital contributions

$$p_{ij} = \sum_{n} p_{ij}^{n} \quad (i \neq j), \tag{2.8}$$

where

$$p_{ij}^{n} = N_n T_{in} T_{jn}. \tag{2.9}$$

The quantities p_{ij}^{n} ($i =$ and $\neq j$) contain all the information that is contained in the quantities p_{ij}, N_n, and T_{in}. This FORS population-bond-order analysis implements the conceptual objectives of Mulliken's analysis *in terms of a basis-set independent formalism* with a non-arbitary *intrinsic* population definition that, moreover, does not suffer from the kind of problems illustrated, e.g., in Fig. 4 on p. 37 of [5b].

The interpretative significance of the natural orbitals derives from the fact that they furnish a division of the molecular orbitals into strongly occupied ones, which reveal "where the action is", and into weakly occupied ones which are required to provide the wavefunction with the flexibility to describe what are generally considered the effects of electron correlation. It is the FORS population analysis of the *strongly* occupied molecular orbitals that would correspond to Mulliken's population analysis [5] of self-consistent-field wavefunctions where all MOs are natural orbitals with occupation number 2. The FORS population analysis provides in addition a complementary analysis of the correlating orbitals.

In Sect. 5 we shall find that, in some cases, a third set of FORS molecular orbitals is useful to facilitate chemical insight. They are the FORS analogues to the traditional localized SCF orbitals [6] and are obtained by localizing the *strongly* occupied FORS MOs and the *weakly* occupied FORS MOs *separately*. The resulting molecular orbitals still yield quite small off-diagonal density matrix elements and, hence, are still near-natural orbitals. They combine the separation into strong and weakly occupied orbitals with the localization into regions of chemical interest. For this reason we shall call them *chemically localized* FORS

MOs (as contrasted to the *atom-localized* quasi-atomic FORS MOs). In [3b] they were called chemically adapted FORS MOs. Sometimes it is illuminating to formulate the population and bond order analysis in terms of these orbitals.

2.3. *Configurational analysis of a FORS wavefunction*

The *configurations* which are generated by the localized FORS MOs are also instructive. Since the localized MOs have the character of molecule-adapted minimal-basis atomic orbitals, the configurations generated by them have the formal appearance of *valence-bond structures between quasi-atomic orbitals.* In the case at hand, they are spin-adapted antisymmetrized products (SAAPs) which look like valence bond structures between the localized reactive FORS MOs $|0\rangle$, $|0'\rangle$, $|1\rangle$, $|2\rangle$ of Fig. 1. They form three groups: Four neutral configurations which have the formal appearance of covalent VB structures:

$$C_0^0 C_1^0 C_2^0: \quad |0^2 12\rangle, |0'^2 12\rangle, |00'12S\rangle, |00'12T\rangle$$

where S and T imply the four-electron singlet and triplet spin couplings; fourteen "singly-ionic" configurations:

$$\begin{aligned}
C_1^- C_2^+: &\quad |0^2 1^2\rangle, |0'^2 1^2\rangle, |00'1^2\rangle \\
C_1^+ C_2^-: &\quad |0^2 2^2\rangle, |0'^2 2^2\rangle, |00'2^2\rangle \\
C_0^+ C_1^-: &\quad |021^2\rangle, |0'21^2\rangle \\
C_0^- C_1^+: &\quad |0^2 0'2\rangle, |0'^2 02\rangle \\
C_0^+ C_2^-: &\quad |012^2\rangle, |0'12^2\rangle \\
C_0^- C_2^+: &\quad |0^2 0'1\rangle, |0'^2 01\rangle;
\end{aligned}$$

and two "doubly-ionic" configurations:

$$C_0^{2-} C_1^+ C_2^+: \quad |0^2 0'^2\rangle, \qquad C_0^{2+} C_1^- C_2^-: \quad |1^2 2^2\rangle.$$

The explicit forms of the listed wavefunctions (SAAPs) are defined in Sect. 2.1 of [1]. The orbital symbols and the numbering of atoms are apparent from Fig. 1.

The physical meaning and chemical interpretation of these SAAPs differ, however, significantly from that of traditional VB structures because, their quasi-atomic character notwithstanding, the localized FORS MOs are mutually orthogonal and so are therefore the SAAPs constructed from them.

While it is still true that, in the case of nonpolar bonding, such as encountered here, the dominant configuration Ψ_0 is a SAAP which looks like a covalent VB structure, it is readily seen that this configuration embodies *no interference (resonance) interactions* between the quasi-atomic localized FORS orbitals when the latter are orthogonal. Its energy contains only *intra-atomic deformation energies and those interatomic effects which arise from non-bonded repulsions and coulombic interactions.* We therefore call it "neutral" (i.e., without charge transfer) or "unshared" rather than "covalent".

Electron-sharing between atoms results from the admixture of additional configurations Ψ_{+-} which have the formal appearance of ionic VB structures. They describe electrons moving back and forth between the orthogonal molecule-adapted quasi-atomic orbitals on different atoms. It is these "electron jumps" which lead to chemical bonding because it is found that *the essential, energy lowering interference (resonance) terms $p_{ij}\langle i|h|j\rangle$ are embedded in the*

interaction matrix elements $\langle \Psi_0 | H | \Psi_{+-} \rangle$. *The magnitudes of the coefficients of these electron-hopping configurations provide therefore an indication of where bonds are established* so that inferences can be drawn from the FORS-CI expansion. These matters will become clearer by an examination of the specific cases.

On the other hand, the configurations in terms of the *natural* MOs have the well-known property of *compacting* the configurational expansion. In general they can be grouped into "principal" configurations of the SCF type and "secondary" configurations providing electron correlation for the former.

2.4. The localization process

Since the localization of FORS MOs into quasi-atomic form is a fundamental prerequisite of the present analysis, it requires further comment.

An analysis such as the one developed here is useless unless the entire procedure is basis-set independent. In order to establish this independence we have performed the analysis for the minimal-basis-set calculation of [1] as well as for more accurate calculations with extended basis sets whose details are described in the subsequent paper [2]. The results of the former analysis are discussed in Sects. 3–5; the results of the latter analysis are discussed in Sect. 6. The comparison of the two analyses establishes (i) that it is in fact possible to localize FORS MOs into quasi-atomic form, in agreement with the conclusions of our earlier investigations [3b] and (ii) that these quasi-atomic MOs are indeed basis-set-independent orbitals which are *intrinsic to the wavefunction.*

In the present investigation, all localizations were accomplished with the Edmiston–Ruedenberg procedure [6]. However, since it is now established that the localized FORS MOs have quasi-atomic character, it would seem desirable in future applications *to maximize this atomic character.* One way to do this is to maximize the projection of these MOs on the orbital space spanned by the relevant (core and/or valence) SCF or MCSCF orbitals of the free atoms. If $\phi_1, \phi_2, \ldots, \phi_M$ is a set of molecular FORS MOs and if the free-atom orbitals for a particular atom are $\chi_1, \chi_2, \ldots, \chi_A$, $(A < M)$, then the solution of the eigenvalue equation:

$$\sum_n^M L_{mn} T_{nv} = \lambda_v T_{mv}$$

with

$$L_{mn} = \sum_\alpha^A \langle \phi_m | \phi_\alpha \rangle \langle \phi_\alpha | \phi_n \rangle, \quad m, n = 1, 2, \ldots, M,$$

for the $\hat{A}$ largest values of λ_v, will yield the coefficients T_{nv} such that the $\hat{A}$ FORS MOs:

$$\hat{\phi}_v = \sum_n^M \phi_n T_{nv}, \quad v = 1, 2, \ldots, \hat{A}$$

are those with the largest projections on the space spanned by the atomic orbitals $\chi_1, \chi_2, \ldots, \chi_A$. The $\hat{\phi}_v$ from different atoms have then to be symmetrically orthogonalized. The number $\hat{A}$ of orbitals assigned to each atom should be chosen so as to maximize the sum of the projections on all atoms. Not only does this localization method seem more appropriate for the present purpose, but it is also easier to carry out than the Edmiston–Ruedenberg procedure. The projections

calculated in Sect. 6.1 (see Table 17) indicate that the two localization procedures give very similar results in the present case. Another, energy-based localization procedure will be described elsewhere [7].

3. The ring-opening barrier

3.1. Quasi-atomic FORS MOs

In order to gain insight into the origin of the barrier, we consider the wavefunctions for the geometry of the reactant and for that of the transition state.

Reactant. For cyclopropylidene, one of the reactive natural MOs has B_2 symmetry and it is already localized on the central carbon. *It corresponds to the* π*-orbital* $|0'\rangle$ *of Fig. 1.* We therefore applied the localization only to the three natural MOs of A_1 symmetry and this procedure yields *orbitals corresponding to* $|0\rangle, |1\rangle, |2\rangle$ *of Fig. 1.* Contours of these four localized reaction orbitals as well as of the localized core orbitals mentioned in Sect. 2.1, corresponding to the six sigma bonds, are depicted in panels A to F of Fig. 2. The contours for the CC bonds (shown on panel A) and for the reactive orbitals $|1\rangle$, $|2\rangle$ (shown on panel D) are drawn in the CCC plane. The contours of the orbitals $|0\rangle$ (panel E) and $|0'\rangle$ (panel F) are drawn in the symmetry plane perpendicular to the CCC plane. The contours for any two CH bonds on the same side of the CCC plane are also shown on one panel (panels B or C) and drawn in the plane containing the carbon atoms C_1, C_2, and the two hydrogen atoms. The bonding character of the sigma bonding MOs and the non-interactive character of the orbitals $|0\rangle$ and $|0'\rangle$ are apparent. It is moreover seen that the orbitals $|1\rangle$ and $|2\rangle$ have the character of two strongly overlapping atomic orbitals which can establish a bond between them. We reiterate that the four localized reactive orbitals $|0\rangle$, $|0'\rangle$, $|1\rangle$, $|2\rangle$, their manifestly atomic nature notwithstanding are in fact mutually orthogonal optimized molecular orbitals of the FORS wavefunction. They are *molecular orbitals which have the character of molecule-adapted deformed atomic orbitals, i.e., they are quasi-atomic MOs.*

The drawings also contain the projections of the molecular skeleton on the plane in which the orbital is drawn. Therefore, in panels E and F one can see the inclinations of the CH bonds with respect to the CCC ring which appears as a line. These inclinations are just the inclinations of the planes in which the contours of panels B and C are drawn. The CCC ring therefore appears as a triangle of these panels. It is also apparent that *the orbital* $|1\rangle$ *on atom* C_1 *points in the direction of one member of a roughly tetrahedral hybrid AO quadruple whose other three members point in the bend-bond directions towards the neighboring atoms* H_1, H_2, C_0 (see Figs. 1 and 2 of [1] for the numbering of atoms). The analogous statement is true for the orbital $|2\rangle$ on C_2.

Transition state. In choosing the transition state geometry, we have to keep in mind that, in order to establish the basis-set independence of the analysis, the results for the calculations of [1] must be compared with those for the more accurate calculations of the subsequent paper. For the latter the transition state has however C_s symmetry while the former yielded two transition states of C_1 symmetry with a very flat surface between them. Since we found in Sect. 6.1 of [1] that the point halfway between these two transition states lies only 0.2 kcal/mol higher and, moreover, *has* C_s *symmetry*, we chose to carry out the analysis

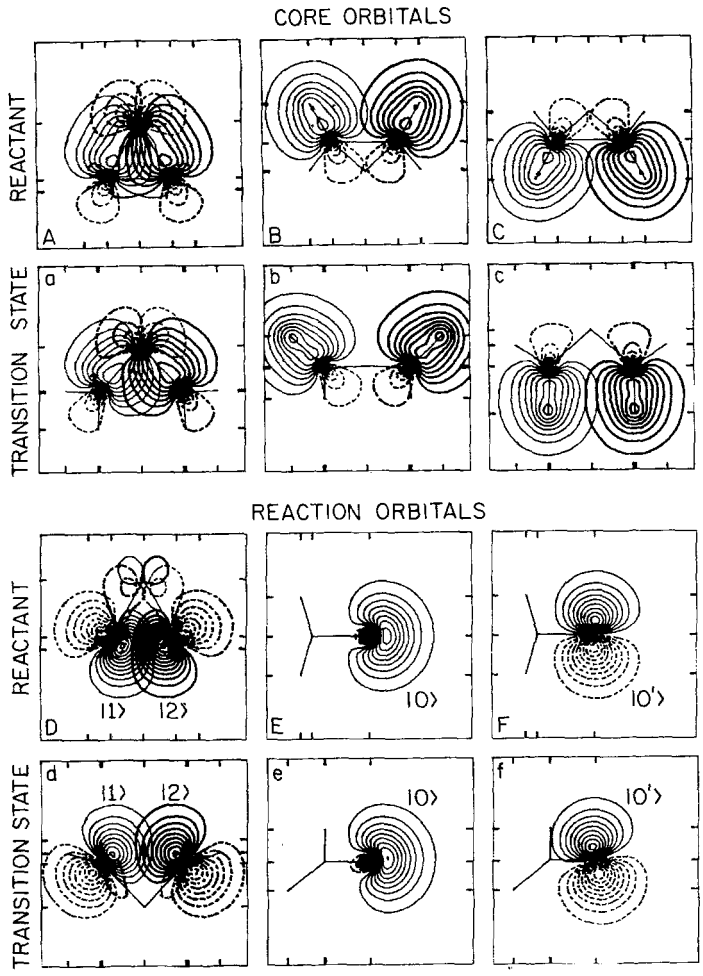

Fig. 2. Quasi-atomic FORS MOs for cyclopropylidene (*panels A to F*) and for the averaged transition state (*panels a to f*). *Solid lines* = positive; *dashed lines* = negative

for the minimal basis set calculation of [1] at this "average transition state" with the coordinates $\Phi = 84.25°$, $\delta_1 = 51.15°$, $\delta_2 = 128.85°$.

Although the CCC plane is no longer a plane of symmetry for this geometry, there still exists an orbital on the central carbon which has essentially π character. We dealt with this problem as follows. First we determined the localized orbitals in the space of all four reaction orbitals and this gave the orbitals $|1\rangle$ and $|2\rangle$ as well as two orbitals on the central carbon which were of the familiar "rabbit-ear" type, as found, e.g., on oxygen in H_2O. We then simply formed the normalized sum and difference of the two rabbit-ear orbitals to yield $|0\rangle$ and $|0'\rangle$. Contours for these orthogonal localized FORS MOs are shown in Fig. 2 on panels a to f opposite the corresponding orbitals of the reactant.

From panels e and f we see that the non-interacting orbitals on the central carbon are now somewhat tilted. By combining the projective views of the CH bonds given on panels b and e one can visualize the direction of the CH bonds

above the CCC plane in three dimensions. By doing the same for panel c and e we can visualize the directions of the CH bonds below the CCC plane. As before, the contours in panels b and c are drawn in the respective planes containing all four bonded atoms. The direction of orbital $|1\rangle$ can again be estimated by imagining it to be the fourth orbital of an approximately tetrahedral hybrid AO quadruple on the carbon C_1, with the other three hybrid AOs pointing towards the three bonded neighbor atoms H_1, $H_{1'}$, C_0 (see Figs. 1 and 2 of [1] for the numbering of atoms). The analogous statement holds for orbital $|2\rangle$. The projection of the central carbon atom on panel d indicates that $|1\rangle$ and $|2\rangle$ both point somewhat above the CCC plane. The actual angle of elevation is 21.4°.

3.2. Population and bond order analysis

Reactant. The density matrices between the four localized reaction orbitals just discussed are listed in Table 1A for the reactant cyclopropylidene. From it, we can draw the following inferences.

Since the diagonal elements, which represent the occupation numbers of the quasi-atomic orbitals, are exactly unity for the orbitals $|1\rangle$ and $|2\rangle$, and sum to exactly 2 for the orbitals $|0\rangle$ and $|0'\rangle$, *there is no interatomic charge transfer between the atoms.* From the off-diagonal elements, which are the bond orders, a strong bonding interaction is inferred to exist between orbitals $|1\rangle$ and $|2\rangle$, which closes the ring in cyclopropylidene. The orbital $|0\rangle$ is a lone pair, it has only a very slight non-bonded repulsion with respect to orbitals $|1\rangle$ and $|2\rangle$. The fact that the bond order between $|0\rangle$ and $|0'\rangle$ is zero implies that the slight occupation of orbital $|0'\rangle$ is entirely due to two-electron interactions, i.e., it serves to correlate the motions of the electrons in orbital $|0\rangle$.

These inferences are confirmed and illustrated in a different way through the natural FORS MOs which diagonalize the density matrix. Each column in Table 2 lists *the expansion coefficients of one natural FORS MO in terms of the*

Table 1. Occupation numbers and bond orders for the reactive quasi-atomic FORS MOs of the reactant and of the averaged transition state

A. Density matrix elements p_{ij} of reactant (cyclopropylidene)

	$\|0\rangle$	$\|0'\rangle$	$\|1\rangle$	$\|2\rangle$
$\|0\rangle$	1.93086	0	−0.00383	−0.00383
$\|0'\rangle$	0	0.06899	0	0
$\|1\rangle$	−0.00383	0	1.00008	0.97114
$\|2\rangle$	−0.00383	0	0.97114	1.00008

B. Density matrix elements p_{ij} of averaged transition state

	$\|0\rangle$	$\|0'\rangle$	$\|1\rangle$	$\|2\rangle$
$\|0\rangle$	1.95653	0.07416	−0.02901	−0.02901
$\|0'\rangle$	0.07416	0.33098	0.46349	0.46349
$\|1\rangle$	−0.02901	0.46349	0.85625	0.71324
$\|2\rangle$	−0.02901	0.46349	0.71324	0.85625

Table 2. Natural FORS MOs for reactant and averaged transition state

A. Cyclopropylidene	$\|lp\rangle$	$\|lpc\rangle$	$\|12b\rangle$	$\|12c\rangle$
$\|0\rangle$	0.991418	0	−0.130730	0
$\|0'\rangle$	0	1	0	0
$\|1\rangle$	0.092440	0	0.701038	0.707107
$\|2\rangle$	0.092440	0	0.701038	−0.707107
N_n	1.930145	0.068991	1.971927	0.028937
Sum	1.999136		2.000864	
B. Averaged transition state	$\|lp\rangle$	$\|lpc\rangle$	$\|10'2b\rangle$	$\|10'2c\rangle$
$\|0\rangle$	0.996130	−0.044076	0.076035	0
$\|0'\rangle$	0.010221	0.917379	0.397883	0
$\|1\rangle$	−0.061723	−0.279708	0.646493	0.707107
$\|2\rangle$	−0.061723	−0.279708	0.646493	−0.707107
N_n	1.960883	0.044782	1.851327	0.143008
Sum	2.005665		1.994335	

quasi-atomic localized FORS MOs $|0\rangle, |0'\rangle, |1\rangle, |2\rangle$. From these expansion coefficients and from the occupation numbers listed in the last two rows, the character of each natural FORS MO is apparent.

In the reactant (Table 2A) nearly two electrons occupy the natural orbital in the first column. Since it consists to 98% of the quasi-atomic σ orbital $|0\rangle$, it essentially describes a σ lone pair on the central carbon and is denoted by $|lp\rangle$. Similarly, nearly two electrons occupy the natural orbital in the third column. Since it consists to 98% of the in-phase linear combination of the quasi-atomic orbitals $|1\rangle$ and $|2\rangle$ it essentially describes a bonding electron pair between the end carbons and is denoted by $|12b\rangle$. The weakly occupied natural orbital in the second column consists entirely of the quasi-atomic π-orbital $|0'\rangle$ which has a node in the region of the lobe of $|lp\rangle$. It thus provides out-of-plane correlation for the lone electron pair in the natural orbital $|lp\rangle$ and it is therefore denoted by $|lpc\rangle$. Similarly, the weakly occupied natural orbital in the fourth column consists of the antibonding linear combination of the quasi-atomic orbitals $|1\rangle$ and $|2\rangle$ which have a node in the region of the lobe of $|12b\rangle$. It thus provides left-right correlation for the bonding electron pair in the natural orbital $|12b\rangle$ and it is therefore called $|12c\rangle$. With the inclusion of the correlation orbitals there are exactly two electrons on C_0 and another two electrons in the C_1C_2 bond.

It should be noted that, since the transformations listed in Table 2 are orthogonal, they can also be read in the inverse directions, i.e., they also represent the expansion of the quasi-atomic orbitals in terms of the natural orbitals. Thus, e.g., the orbital $|1\rangle$ results from linearly superposing the natural orbitals $|lp\rangle$, $|12b\rangle$, and $|12c\rangle$ with the coefficients listed in the *row* headed by the label $|1\rangle$.

The conclusions inferred for the populations from the localized and the natural representations can be intelligibly combined by means of the quantities

Table 3. FORS population analysis for reactant and averaged transition state

A. Cyclopropylidene

		Natural FORS MOs					
		$\|lp\rangle$	$\|lpc\rangle$	$\|12b\rangle$	$\|12c\rangle$	p_{ii}	Atoms
Quasi-	$\|0\rangle$	1.89716	0	0.03370	0	1.93086	1.99985
atomic	$\|0'\rangle$	0	0.06899	0	0	0.06899	
FORS	$\|1\rangle$	0.01649	0	0.96911	0.01447	1.00007	1.00007
MOs	$\|2\rangle$	0.01649	0	0.96911	0.01447	1.00007	1.00007
	N_n	1.93015	0.06899	1.97193	0.02894		
	Sum	1.99914		2.00086		4	4

B. Averaged transition state

		Natural FORS MOs					
		$\|lp\rangle$	$\|lpc\rangle$	$\|10'2b\rangle$	$\|10'2c\rangle$	p_{ii}	Atoms
Quasi-	$\|0\rangle$	1.94574	0.00009	0.01070	0	1.95653	2.28750
atomic	$\|0'\rangle$	0.00020	0.03769	0.29309	0	0.33098	
FORS	$\|1\rangle$	0.00747	0.00350	0.77377	0.07150	0.85624	0.85624
MOs	$\|2\rangle$	0.00747	0.00350	0.77377	0.07150	0.85624	0.85624
	N_n	1.96088	0.04478	1.85133	0.14301		
	Sum	2.00566		1.99434		4	4

$p_{ii}^n = N_n T_{in}^2$ which were defined by Eq. (2.6) of Sect. 2.2. This approach leads to the summary population analysis given in Table 3A. The quantities p_{ii}^n form the center bloc. Each column adds up to the value in the row labeled N_n, i.e., the populations of the natural orbitals. Each row adds up to the value in the column labeled p_{ii}, i.e., the populations of the quasi-atomic orbitals. Thus, the p_{ii}^n yield an atomic breakdown of the natural orbital population as well as a natural-orbital breakdown of the atomic populations—as expressed by Eqs. (2.7) of Sect. 2.2. The table shows that the population in the σ quasi-atomic orbital $|0\rangle$ essentially comes from the lone pair natural orbital $|lp\rangle$ and that the populations of $|1\rangle$ and $|2\rangle$ come essentially from the bonding orbital $|12b\rangle$. It furthermore shows how the smaller population contributions due to correlation as well as orbital delocalization round out the total population picture. Thus the naive qualitative reasoning, while correct in principle, must be tempered in two respects in order to fit in with the quantitative *ab-initio* analysis: First, the concept of a pure atomic orbital must be replaced by that of a deformed quasi-atomic orbital. Secondly, even these deformed atomic orbitals get slightly mixed when the natural orbitals are formed which describe the lone pair, bonding and correlation roles of electrons.

The corresponding bond order decomposition in terms of natural orbital contributions, corresponding to Eqs. (2.8) and (2.9) of Sect. 2.2 is given in Table 4A. It shows that the bond order between $|1\rangle$ and $|2\rangle$ arises essentially from the bonding orbital $|12b\rangle$.

Transition state. The density matrix of the transition state in Table 1B shows that there has occurred a substantial charge transfer from the end carbons to the

Table 4. FORS bond order analysis for reactant and averaged transition state

A. Cyclopropylidene

		Natural FORS MOs				
		$\|lp\rangle$	$\|lpc\rangle$	$\|12b\rangle$	$\|12c\rangle$	p_{ij}
Quasi-	(00′)	0	0	0	0	0
atomic	(01)	0.17689	0	−0.18072	0	−0.00383
FORS	(02)	0.17689	0	−0.18072	0	−0.00383
MO	(0′1)	0	0	0	0	0
pairs	(0′2)	0	0	0	0	0
	(12)	0.01649	0	0.96911	−0.01447	0.97113

B. Averaged transition state

		Natural FORS MOs				
		$\|lp\rangle$	$\|lpc\rangle$	$\|10'2b\rangle$	$\|10'2c\rangle$	p_{ij}
Quasi-	(00′)	0.01996	−0.00181	0.05601	0	0.07416
atomic	(01)	−0.12056	0.00055	0.09100	0	−0.02901
FORS	(02)	−0.12056	0.00055	0.09100	0	−0.02901
MO	(0′1)	−0.00124	−0.01149	0.47621	0	0.46348
pairs	(0′2)	−0.00124	−0.01149	0.47621	0	0.46348
	(12)	0.00747	0.00350	0.77377	−0.07150	0.71324

central carbon atom. Each of the orbitals $|1\rangle$ and $|2\rangle$ has given up 0.1438 electrons. Almost all of the total amount of 0.2877 electrons, namely 0.2620 electrons, has been donated to the orbital $|0'\rangle$ on the central carbon; only 0.0257 has gone to $|0\rangle$. The substantial positive bond orders between the orbitals $|0'\rangle$, $|1\rangle$, $|2\rangle$ imply that we have an in-phase three-center delocalization of the two electrons which, in the reactant, formed the $|1\rangle-|2\rangle$ bond. The reason must be that, due to the increase in distance between the end carbons (from 1.53 to 1.94 Å; see Table 1 of [1]), the interaction between $|1\rangle$ and $|2\rangle$ has considerably weakened and, as a consequence, the orbitals $|1\rangle$ and $|2\rangle$ have rotated in order to strengthen their interactions with the closer orbital $|0'\rangle$. This accounts for the rotations of the hydrogen atoms as well as for the tilting of the $|0'\rangle$ orbital evident in Fig. 2f. The relatively large bond order between orbitals $|1\rangle$ and $|2\rangle$ is the consequence of the in-phase $|1\rangle-|0'\rangle-|2\rangle$ delocalization and does not imply a strong direct $|1\rangle-|2\rangle$ bond since the resonance integral $\langle 1|h|2\rangle$ is presumably small. The energetic gain obtained from the establishment of the delocalized three-center bond $|1\rangle-|0'\rangle-|2\rangle$ is of course partly offset by the need for substantial electron donation to the central carbon which clearly does not come free. Thus, we conclude that the energy barrier results from the breakage of the $|1\rangle-|2\rangle$ bond and that its smallness results from the establishment of the three-center bond through electron donation into the previously empty orbital $|0'\rangle$.

The natural orbital $|lp\rangle$ of the first column of Table 2B still describes a lone electron pair essentially lodged in the quasi-atomic σ-orbital $|0\rangle$ on the center atom. The major change compared to cyclopropylidene is the in-phase delocalization of the bonding natural orbital of the third column of Table 2B over the quasi-atomic π-orbital $|0'\rangle$ of the central atom. We have therefore labeled it

$|10'2b\rangle$. The natural orbital $|lpc\rangle$ of the second column is still essentially the quasi-atomic π-orbital $|0'\rangle$, but it is somewhat delocalized over the orbitals $|1\rangle$ and $|2\rangle$ in an out-of-phase (antibonding) fashion. This orbital therefore still essentially provides out-of-phase correlation for the lone pair natural orbital $|lp\rangle$, but it also provides some bond-parallel correlation for the three-center bond orbital $|10'2b\rangle$. The major bond-parallel correlation for this three-center bond still comes from the natural orbital $|10'2c\rangle$ which, in fact, has a higher occupancy than it had in cyclopropylidene.

The information from the localized and natural density decompositions is again integrated in the form of a population analysis and a bond order analysis in Tables 3B and 4B. The comparison of these tables with Tables 3A and 4A reconfirms that the bonding orbital $|10'2b\rangle$ has now delocalized its population over the π-orbital $|0'\rangle$ on the central carbon. Its correlating orbital $|10'2c\rangle$ has increased its population sevenfold presumably because, due to the longer C_1-C_2 distance, it is now much less antibonding and therefore more effective for correlation. The usage of the atomic orbital $|0'\rangle$ for delocalized bonding in the natural orbital $|10'2b\rangle$ has conversely induced an antibonding delocalization of the correlating orbital $|lpc\rangle$ over the atomic orbitals $|1\rangle$ and $|2\rangle$. Thereby it has become less effective for correlating the lone pair orbital $|lp\rangle$ which has concentrated more on the quasi-atomic σ-orbital $|0\rangle$. The fact that this orbital on the central carbon is still essentially doubly occupied indicates that its energy is still sufficiently below that of the quasi-atomic π-orbital $|0'\rangle$.

3.3. FORS configurational analysis

We now examine the configurations (SAAPs = spin-adapted antisymmetrized products) which are generated by the discussed localized FORS MOs. They are listed, in the order discussed in Sect. 2.3, in the first column of Table 5. The second column contains the corresponding expansion coefficients for the wavefunction of the reactant; the third column contains the wavefunction expansion coefficients for the molecule at the considered approximate transition state. Although the qualitative meaning of the configurations is the same, the orbitals are of course quantitatively different in the two cases as shown in Fig. 2.

Reactant. For the reactant the dominant configuration is the SAAP $|0^2 12\rangle$ corresponding to a sigma lone pair on C_0 and one reaction electron each on C_1 and C_2. The SAAP $|0'^2 12\rangle$ clearly provides electron correlation for the sigma lone pair. We therefore consider:

$$\Psi_B = 0.9827|0^2 12\rangle - 0.1855|0'^2 12\rangle$$

as the normalized neutral *base function without electron sharing* (see Sect. 2.3). It has a weight of 62% in the wavefunction. The double occupation of the σ-orbital $|0\rangle$ is due to the fact that, for such small CCC opening angle, the π-atomic orbital $|0'\rangle$ has a significantly higher orbital energy.

As explained above in Sect. 2.3, the base function Ψ_B by itself does not establish a bond between the orbitals $|1\rangle$ and $|2\rangle$. In the present case, covalent bonding arises from the admixture of the SAAPs $|0^2 1^2\rangle$ and $|0^2 2^2\rangle$ which, together with the SAAPs $|0'^2 1^2\rangle$ and $|0'^2 2^2\rangle$ practically account for the remaining 38% of the wavefunction. It is readily verified that these terms can be generated

Table 5. Expansion coefficients of wavefunctions for cyclopropylidene and the averaged transition state in terms of configurations generated from quasi-atomic FORS MOs

SAAPs		Cyclopropylidene	Transition state
$C_0^0C_1^0C_2^0$:	$\|0^212\rangle$	0.772606	0.746158
	$\|0'^212\rangle$	−0.145750	−0.124982
	$\|00'12S\rangle$	0	0.046221
	$\|00'12T\rangle$	0	0
$C_1^-C_2^+$:	$\|0^21^2\rangle$	0.429145	0.265866
	$\|0'^21^2\rangle$	−0.081054	−0.041151
	$\|00'1^2\rangle$	0	0.029490
$C_1^+C_2^-$:	$\|0^22^2\rangle$	0.429145	0.265866
	$\|0'^22^2\rangle$	−0.081054	−0.041151
	$\|00'2^2\rangle$	0	0.029490
$C_0^-C_1^+$:	$\|0^20'2\rangle$	0	0.365665
	$\|0'^202\rangle$	0.007386	−0.020085
$C_0^+C_1^-$:	$\|021^2\rangle$	0.011068	0.019080
	$\|0'21^2\rangle$	0	0.003320
$C_0^-C_2^+$:	$\|0^20'1\rangle$	0	0.365665
	$\|0'^201\rangle$	0.007386	−0.020085
$C_0^+C_2^-$:	$\|012^2\rangle$	0.011068	0.019080
	$\|0'12^2\rangle$	0	0.003320
$C_0^{2-}C_1^+C_2^+$:	$\|0^20'^2\rangle$	−0.001957	0.100078
$C_0^{2+}C_1^-C_2^-$:	$\|1^22^2\rangle$	−0.003294	−0.001356

in just the right proportion from the base function Ψ_B by the substitution operations:

$$R_{1\to 2}\Psi_B = 0.982|0^22^2\rangle - 0.185|0'^22^2\rangle,$$

$$R_{2\to 1}\Psi_B = 0.982|0^21^2\rangle - 0.185|0'^21^2\rangle,$$

where the orbital replacement operator $R_{i\to j} = \{|i\rangle \to |j\rangle\}$ can be interpreted as allowing an electron to jump from orbital $|i\rangle$ to orbital $|j\rangle$. As discussed in Sect. 2.3, the admixture of these configurations introduces into the wavefunction electron sharing between the orthogonal orbitals $|1\rangle$ and $|2\rangle$ and, as a consequence, there occurs an energy lowering due to the interference terms in the hamiltonian matrix elements between Ψ_B and $R_{1\to 2}\Psi_B$, $R_{2\to 1}\Psi_B$. It is this energy lowering which establishes the bond between orbitals $|1\rangle$ and $|2\rangle$.

Transition state. For the transition state we find from the third column of Table 5 the very similar normalized base function without electron sharing:

$$\Psi_B = 0.986|0^212\rangle - 0.165|0'^212\rangle$$

which here has a weight of 57%. In this case the substituted configurations $R_{1\to 2}\Psi_B$ and $R_{2\to 1}\Psi_B$ account, however, for only 15% of the wavefunction, which indicates that electron sharing between $|1\rangle$ and $|2\rangle$ is energetically much less profitable, undoubtedly because of the greater distance between the carbon

atoms 1 and 2. The remaining 28% are mainly due to configurations that describe electron sharing between C_1, C_2, and the central atom C_0, notably:

$$|0^20'2\rangle = R_{1\to 0'}|0^212\rangle,$$
$$|0^20'1\rangle = R_{2\to 0'}|0^212\rangle.$$

These SAAPs describe electron donation from $|1\rangle$ and $|2\rangle$ to the previously empty quasi-atomic π-orbital $|0'\rangle$ on the central atom and therefore a delocalization of electrons from orbital $|1\rangle$ over orbital $|0'\rangle$ to orbital $|2\rangle$.

The comparison of the wavefunction expansion of the reactant with that of the transition state thus shows again that the existence of the barrier is due to the loss of the covalent binding between the orbitals $|1\rangle$ and $|2\rangle$, and that its small value is related to a compensating energy lowering which arises from delocalization of the same two electrons over the orbitals $|1\rangle$, $|0'\rangle$, $|2\rangle$.

4. The allene isomerization barrier

In order to gain insight into the energy barrier to the isomerization of singlet allene, we examine the wavefunctions for the staggered linear equilibrium conformation and for the planar, bent ($\Phi = 133°$) transition state. No orbital plots are displayed since, from what has been seen before, the shapes and directions of the localized FORS MOs are manifestly as drawn in Fig. 1. For the linear conformation, $|1\rangle$ and $|0\rangle$ are parallel quasi-atomic p-orbitals whereas $|0'\rangle$ and $|2\rangle$ are parallel quasi-atomic p-orbitals at right angles to $|1\rangle$ and $|0\rangle$. For the bent planar geometry, the orbitals $|1\rangle$, $|2\rangle$ and $|0'\rangle$ are quasi-atomic p-orbitals perpendicular to the molecular pane whereas $|0\rangle$ is a quasi-atomic s-p hybrid-type orbital in the molecular plane pointing "backwards", i.e., away from the end carbons.

4.1. Staggered linear allene

The density matrix for the quasi-atomic FORS MOs is listed in Table 6A. It is apparent that bonding exists between orbitals $|0\rangle$ and $|1\rangle$ as well as between

Table 6. Occupation numbers and bond orders for the reactive quasi-atomic FORS MOs of linear and bent allene

A. Density matrix elements p_{ij} of product (linear allene)

p_{ij}	$\|0\rangle$	$\|0'\rangle$	$\|1\rangle$	$\|2\rangle$
$\|0\rangle$	0.94821	0	0.88684	0
$\|0'\rangle$	0	0.94821	0	0.88684
$\|1\rangle$	0.88684	0	1.05179	0
$\|2\rangle$	0	0.88684	0	1.05179

B. Density matrix elements p_{ij} of bent allene

p_{ij}	$\|0\rangle$	$\|0'\rangle$	$\|1\rangle$	$\|2\rangle$
$\|0\rangle$	1.00000	0	0	0
$\|0'\rangle$	0	0.97708	0.59743	0.59743
$\|1\rangle$	0	0.59743	1.01146	0.01146
$\|2\rangle$	0	0.59743	0.01146	1.01146

Table 7. Natural FORS MOs for linear and bent allene

A. Linear allene	$\|01b\rangle$	$\|01c\rangle$	$\|0'2b\rangle$	$\|0'2c\rangle$
$\|0\rangle$	0.686185	0.727427	0	0
$\|0'\rangle$	0	0	0.686185	0.727427
$\|1\rangle$	0.727427	−0.686185	0	0
$\|2\rangle$	0	0	0.727427	−0.686185
N_n	1.888351	0.111649	1.888351	0.111649
Sum	2.000000		2.000000	

B. Bent allene	$\|lp\rangle$	$\|12n\rangle$	$\|10'2b\rangle$	$\|10'2c\rangle$
$\|0\rangle$	1	0	0	0
$\|0'\rangle$	0	0	0.697454	0.716629
$\|1\rangle$	0	0.707107	0.506733	−0.493175
$\|2\rangle$	0	−0.707107	0.506733	−0.493175
N_n	1.000000	1.000000	1.845206	0.154794
Sum			2.000000	

orbitals $|0'\rangle$ and $|2\rangle$. Concomitantly charge in the amount of 0.05 electrons is transferred from $|0\rangle$ to $|1\rangle$ and similarly from $|0'\rangle$ to $|2\rangle$. Table 7A lists the natural orbitals. For each of the two bonds (01) and (0′2) we have one bonding and one correlating orbital. The population and bond order analyses, given in Tables 8A and 9A, quantify the preceding remarks further in a self-explanatory way.

Table 8. FORS population analysis for linear and bent allene

A. Linear allene		Natural FORS MOs					
		$\|01b\rangle$	$\|01c\rangle$	$\|0'2b\rangle$	$\|0'2c\rangle$	p_{ii}	Atoms
Quasi-	$\|0\rangle$	0.88913	0.05908	0	0	0.94821	1.89642
atomic	$\|0'\rangle$	0	0	0.88913	0.05908	0.94821	
FORS	$\|1\rangle$	0.99922	0.05257	0	0	1.05179	1.05179
MOs	$\|2\rangle$	0	0	0.99922	0.05257	1.05179	1.05179
	N_n	1.88835	0.11165	1.88835	0.11165		
	Sum	2.00000		2.00000		4	4

B. Bent allene		Natural FORS MOs					
		$\|lp\rangle$	$\|12n\rangle$	$\|10'2b\rangle$	$\|10'2c\rangle$	p_{ii}	Atoms
Quasi-	$\|0\rangle$	1.00000	0	0	0	1.00000	1.97709
atomic	$\|0'\rangle$	0	0	0.89759	0.07950	0.97709	
FORS	$\|1\rangle$	0	0.5	0.47381	0.03765	1.01146	1.01146
MOs	$\|2\rangle$	0	0.5	0.47381	0.03765	1.01146	1.01146
	N_n	1.00000	1.00000	1.84521	0.15479		
	Sum			2.00000		4	4

Table 9. FORS bond order analysis for linear and bent allene

A. Linear allene

		Natural FORS MOs				
		$\|01b\rangle$	$\|01c\rangle$	$\|0'2b\rangle$	$\|0'2c\rangle$	p_{ij}
Quasi-	(00′)	0	0	0	0	0
atomic	(01)	0.94257	−0.05573	0	0	0.88684
FORS	(02)	0	0	0	0	0
MO	(0′1)	0	0	0	0	0
pairs	(0′2)	0	0	0.94257	−0.05573	0.88684
	(12)	0	0	0	0	0

B. Bent allene

		Natural FORS MOs				
		$\|lp\rangle$	$\|12n\rangle$	$\|10'2b\rangle$	$\|10'2c\rangle$	p_{ij}
Quasi-	(00′)	0	0	0	0	0
atomic	(01)	0	0	0	0	0
FORS	(02)	0	0	0	0	0
MO	(0′1)	0	0	0.65214	−0.05471	0.59743
pairs	(0′2)	0	0	0.65214	−0.05471	0.59743
	(12)	0	−0.5	0.47381	0.03765	0.01146

The configurational expansion coefficients of the wavefunction in terms of the corresponding SAAPs are given in Table 10. The neutral base function without electron sharing is:

$$\Psi_B = 0.997|010'2S\rangle + 0.069|010'2T\rangle.$$

The predominant term is the *singlet* coupled SAAP coupling $|0\rangle$ with $|1\rangle$ and $|0'\rangle$ with $|2\rangle$, embodying the bond between $|0\rangle$ and $|1\rangle$ as well as the bond between $|0'\rangle$ and $|2\rangle$. For the cases to be discussed in Sect. 5 it is not possible to cast Ψ_B in such a form because, in those cases, the Hund's-rule triplet-singlet effect in the central atom is stronger than the weak π-bonding effects so that the triplet effect dominates. Here, in allene, the strong covalent π-bonding effects dominate over the local Hund's-rule effect at the central carbon. Ψ_B contributes 53% to the wavefunction. Table 10 also confirms that covalent bonding is due to electron sharing between the orbitals $|1\rangle$ and $|0\rangle$ and between the orbitals $|2\rangle$ and $|0'\rangle$ as is established by the SAAPs generated from Ψ_B by the electron-hopping replacements $R_{1\to 0}$, $R_{0\to 1}$, $R_{2\to 0'}$, $R_{0'\to 2}$ namely:

$$R_{1\to 0}\Psi_B = |0^2 20'\rangle \qquad R_{2\to 0'}\Psi_B = |0'^2 01\rangle$$

$$R_{0\to 1}\Psi_B = |1^2 20'\rangle \qquad R_{0'\to 2}\Psi_B = |2^2 01\rangle$$

$$R_{1\to 0}R_{2\to 0'}\Psi_B = |0^2 0'^2\rangle \qquad R_{1\to 0}R_{0'\to 2}\Psi_B = |0^2 2^2\rangle$$

$$R_{0\to 1}R_{0'\to 2}\Psi_B = |1^2 2^2\rangle \qquad R_{0\to 1}R_{2\to 0'}\Psi_B = |0'^2 1^2\rangle.$$

Table 10. Expansion coefficients of wavefunctions for linear and bent allene in terms of configurations generated from quasi-atomic FORS MOs

SAAPs		Linear allene	Bent allene
Covalent:	$\|0^2 12\rangle$	0	0
	$\|0'^2 12\rangle$	0	0
	$\|010'2S\rangle$	0.723744	0.722086
	$\|010'2T\rangle$	0.050349	−0.416897
$C_1^- C_2^+$:	$\|0^2 1^2\rangle$	−0.005680	0
	$\|0'^2 1^2\rangle$	0.145391	0
	$\|00'1^2\rangle$	0	0.096605
$C_1^+ C_2^-$:	$\|0^2 2^2\rangle$	0.145391	0
	$\|0'^2 2^2\rangle$	−0.005680	0
	$\|00'2^2\rangle$	0	−0.096605
$C_0^- C_1^+$:	$\|0^2 0'2\rangle$	0.282896	0
	$\|0'^2 02\rangle$	0	0.256518
$C_0^+ C_1^-$:	$\|1^2 02\rangle$	0	0.277958
	$\|1^2 0'2\rangle$	0.344264	0
$C_0^- C_2^+$:	$\|0^2 0'1\rangle$	0	0
	$\|0'^2 01\rangle$	0.282896	−0.256518
$C_0^+ C_2^-$:	$\|2^2 01\rangle$	0.344264	−0.277958
	$\|2^2 0'1\rangle$	0	0
$C_0^{2-} C_1^+ C_2^+$:	$\|0^2 0'^2\rangle$	0.102271	0
$C_0^{2+} C_1^- C_2^-$:	$\|1^2 2^2\rangle$	0.154157	0

4.2. Bent planar allene ($\Phi = 133.3°$)

It is instructive to compare the electronic structure of the bent planar allene transition state ("*all*-TS") not only with the linear staggered allene conformation but also with the averaged ring-opening transition state of cyclopropylidene ("*cyc*-TS") discussed in Sect. 3. Both conformations have the same C_s symmetry plane but they differ in two respects, namely: the *all*-TS has a ring-opening angle $\Phi = 133.3°$ and both CH_2 groups lie in the CCC plane so that the molecule has C_{2v} symmetry, whereas the *cyc*-TS has $\Phi = 84°$ and the CH_2 groups are tilted against the CCC plane so that the symmetry is only C_s.

The population-bond order matrix is listed in Table 6B, the expansions of the natural orbitals in terms of the quasi-atomic orbitals are listed in Table 7B, the population analysis is given by Table 8B and the bond order analysis is given by Table 9B. The corresponding data for the *cyc*-TS were given in Tables 1B, 2B, 3B, 4B. A synoptic examination of the four tables for each of the two transition states leads to the following comparative inferences.

The four natural orbitals are similar for the two transition states, namely (see Tables 2 and 7):

$|a_1\rangle = |lp\rangle \simeq |0\rangle$ is essentially a non-interacting lone orbital on the central carbon;

$|1b_1\rangle = |10'2b\rangle$ is a delocalized bonding orbital with positive contributions from $|1\rangle$, $|0'\rangle$ and $|2\rangle$;

$|2b_1\rangle = |10'2c\rangle$ in the *all*-TS and $\simeq |lpc\rangle$ in the *cyc*-TS, is a delocalized antibonding orbital with a node between $|1\rangle$ and $|0'\rangle$ and another node between $|0'\rangle$ and $|2\rangle$;

$|a_2\rangle = (|1\rangle - |2\rangle)/\sqrt{2}$ has one node and no contribution from the central carbon.

The labels a_1, b_1, a_2 correspond to the respective C_{2v} irreps in the allene transition state. The increase of the CCC angle Φ from 84° to 133° has the following consequences regarding these molecular orbitals:

(i) The $|a_1\rangle$ orbital loses *s*-character and its orbital energy *increases* correspondingly;

(ii) Since the increase in the distance of the end carbons decreases the steric repulsions between the hydrogens, they turn into the plane, allowing for greater π-overlap by lining up the orbitals $|1\rangle$, $|0'\rangle$ and $|2\rangle$. This lowers the orbital energy of $|1b_1\rangle$;

(iii) The increase in distance between $|1\rangle$ and $|2\rangle$ also lowers the antibonding effect between them, thereby lowering the orbital energy of $|a_2\rangle$. In the *cyc*-TS $|a_2\rangle$ is antibonding, but in the *all*-TS $|a_2\rangle$ is nonbonding with diradical character.

Because of these energy changes, the opening from 85° to 133° under preservation of C_s symmetry leads to an essential population shift (see Tables 3 and 8). Since the energy of $|a_1\rangle$ increases, whereas that of $|a_2\rangle$ decreases to a nonbonding level, the occupations change from 1.95 for $|a_1\rangle$ and 0.14 for $|a_2\rangle$ in the *cyc*-TS to unity for *both* orbitals in the *all*-TS, giving it diradical character.

This occupation shift, in turn, changes the character of the $|1b_1\rangle = |10'2b\rangle$ bonding orbital (see Tables 3 and 8). In the *cyc*-TS, its major contributions (0.77 each) are on $|1\rangle$ and $|2\rangle$ with only a small contribution to $|0'\rangle$ representing an electron donation of 0.29 electrons to the center carbon. By contrast, in the *all*-TS the occupation of $|0'\rangle$ does not represent an electron donation, because $|a_1\rangle \simeq |0\rangle$ holds only one electron. Consequently, the orbital $|0'\rangle$ contributes 0.90 to $|10'2b\rangle$ whereas $|1\rangle$ and $|2\rangle$ contribute only 0.47 each. Moreover, because of the occupancy of $|a_2\rangle$ with one electron there still results a slight charge transfer of 0.01 to the end carbons. This is, however, less than the similar transfer of 0.05 in linear allene.

This population analysis explains the bond order changes shown in Tables 4 and 9. The bonding effects are essentially between $|0'\rangle$ and $|1\rangle$ and between $|0'\rangle$ and $|2\rangle$ since the distance between $|1\rangle$ and $|2\rangle$ is large enough so that the (12) bond order probably multiplies a relatively small energy integral in both cases. The bond orders (01) and (02) in the *cyc*-TS are however lower (0.46 each) than those in the *all*-TS (0.60 each) because the latter is more delocalized over $|0'\rangle - |1\rangle - |2\rangle$, as is apparent from the populations. This increase in π-type bond order from the *cyc*-TS to the *all*-TS parallels the corresponding downhill change in the potential energy surface. In both TSs we have one bonding electron pair covering two atom linkages (01) and (02).

In linear allene, by contrast, the lone pair orbital $|lp\rangle \simeq |0\rangle$ has expanded to cover also the twisted end orbital $|1\rangle$ while the bonding orbital $|10'b\rangle$ has contracted to cover only the end orbital $|2\rangle$ (see Table 8). *For each* of the two linkages there exists therefore a bond, with bond order 0.89 (Table 9). This increase in the total bond order accounts for the energy drop to linear allene.

The configurational expansion of the bent allene wavefunction in terms of SAAPs based on quasi-atomic orbitals is given in the last column of Table 10. It is readily verified that the neutral base function without electron sharing can be written as:

$$\Psi_B = (\sqrt{3}|010'2S\rangle - |010'2T\rangle)/2 = |00'12T\rangle, \tag{4.1}$$

because

$$A\{|0\rangle|0'\rangle|1\rangle|2\rangle\Theta_1\} = -A\{|0\rangle|1\rangle|0'\rangle|2\rangle P_{23}\Theta_1\}$$

and

$$P_{23}\Theta_1 = (-\sqrt{3}\Theta_0 - \Theta_1)/2,$$

where Θ_0, Θ_1 are the singlet- and triplet-coupled spin functions defined in Sect. 2.1 of the first paper [1] and P_{23} denotes a permutation between spin coordinates. Equation (4.1) shows again that, in contrast to the ring-opening transition state, the orbitals $|0\rangle$ and $|0'\rangle$ are here both singly occupied. Ψ_B has a weight of 69.5% in the total wavefunction. Electron sharing is established by the electron-hopping replacements:

$$R_{1\to 0'}\Psi_B = |00'0'2T\rangle = -\sqrt{3}/2|0'^202\rangle$$
$$R_{0'\to 1}\Psi_B = |0112T\rangle = -\sqrt{3}/2|1^202\rangle$$
$$R_{2\to 0'}\Psi_B = |00'10'T\rangle = \sqrt{3}/2|0'^210\rangle = -\sqrt{3}/2|0'^201\rangle$$
$$R_{0'\to 2}\Psi_B = |0212T\rangle = \sqrt{3}/2|2^210\rangle = -\sqrt{3}/2|2^201\rangle$$

confirming the delocalized covalent π-bonding between $|1\rangle$, $|0'\rangle$ and $|2\rangle$. These four terms essentially account for the remaining 30.5% of the wavefunction.

The form of the base function Ψ_B is a consequence of the spatial symmetry. From Table 7 it can be inferred that, in terms of the symmetry-adapted natural orbitals, the dominant SAAP is:

$$\Psi_0 = |(10'2b)^2(lp)(12n)\rangle = |(1b_1)^2a_1a_2\rangle \tag{4.2}$$

and it is apparent that this function belongs to the irreducible representation A_2. So does therefore the total wavefunction and, hence, also Ψ_B. In particular, Ψ_B must therefore satisfy $\sigma\Psi_B = -\Psi_B$ for σ being the mirror plane perpendicular to the molecule. Substituting for Ψ_B the expression of Eq. (4.1), we find:

$$\sigma\Psi_B = |00'21T\rangle = A\{(\hat{P}_{34}00'12)\Theta_1\} \tag{4.3}$$

where $\hat{P}_{34}$ is the transposition of the *spatial* coordinates of electrons 3 and 4. From Eq. (4.3) one deduces:

$$\sigma\Psi_B = -A\{00'12P_{34}\Theta_1\} = -A\{00'12\Theta_1\}$$
$$\sigma\Psi_B = -\Psi_B,$$

which is indeed the required relationship. On the other hand, $|00'12S\rangle$ is unacceptable because $\sigma|00'12S\rangle = +|00'12S\rangle$.

4.3. Symmetry considerations, conical intersection between the two transition states

The average ring-opening transition state at 84.25° and the allene isomerization state at 133° both have C_s symmetry. However, the following reasoning shows

that the groundstate wavefunctions at the two transition states belong to different irreducible representations of C_s. From Table 2 it can be seen that, at the ring-opening transition state, the dominant configuration must be one in which the lone pair orbital (*lp*) and the three-center bonding orbital (10′2*b*) are both doubly occupied. Since both have A' symmetry in C_s, the dominant configuration and, hence, the wavefunction itself belong to the irreducible representation A' at this geometry. On the other hand, Table 7 shows that, at the allene isomerization transition state (bent allene), the dominant configuration is one in which the three-center bonding orbital (10′2*b*) is doubly occupied, whereas the lone pair orbital (*lp*) and the non-bonding orbital (12*n*) between C_1 and C_2 are both singly occupied. Since these three orbitals belong to the irreducible representations A', A', A'', respectively, the dominant configuration and, hence, the entire wavefunction belong to the irreducible representation A'' in C_s at this geometry.

From this change in irreducible representations, it can be inferred that, on a path leading from one of these transition states to the other under preservation of C_s symmetry, there exist two states, of A' and A'' symmetry respectively, which cross somewhere between $\phi = 85°$ and 133°. Within the context of the full potential energy surface, this implies the existence of two surfaces which exhibit a *conical intersection*. The implications of this feature will be discussed in detail in the subsequent paper [2].

5. The free internal cogwheel motion

It stands to reason that, for values of Φ which are not much smaller than 180°, motions along lines $\delta_1 + \delta_2 = \text{constant}$ (see Figs. 9 to 15 in [1]) have a similar meaning as they do in allene, i.e., they represent approximate rigid rotations around an axis which goes approximately through the three carbon and it is for this reason that such motions are approximately free. Such an interpretation breaks down, however, when Φ becomes sufficiently small. Indeed, for $\Phi = 140°$ (Fig. 14, [1]) it is seen that a free motion exists *only along the valleys* $\delta_1 + \delta_2 = 90°$, but *not anymore along the ridges* $\delta_1 + \delta_2 \simeq 0°$. This free motion along the valleys persists for Φ values all the way back almost to the transition state (see Figs. 9 to 15 of [1]). As was described in the discussion of the panel for $\Phi = 84°$ (Fig. 9 of [1]), these motions along the valleys correspond to cogwheel-like synchronized disrotatory motions of the two CH_2 groups with a phase lag of 90° (type II, Fig. 4 in [1]). This result could not have been foreseen without an explicit *ab initio* calculation of the entire surface. How can this *isoenergetic shelf* be explained? In order to answer this question we resort again to an analysis in terms of quasi-atomic FORS MOs. *We consider three geometries along the valley floor on the panel for* $\Phi = 100°$ (Fig. 13 of [1]), namely $(\delta_1, \delta_2) = (90°, 0°), (45°, 45°), (0°, 90°)$.

5.1. Quasi-atomic FORS MOs

$(\delta_1, \delta_2) = (90°, 0°)$. For the geometry $(\delta_1 = 90°, \delta_2 = 0°)$ the right CH_2 group lies in the CCC plane and the left CH_2 group stands perpendicular to it, as illustrated in Fig. 3a. The molecule has C_s symmetry *with respect to the CCC plane* and there are two reaction orbitals of A' symmetry and two of A'' symmetry. Localization of the former yields the in-plane orbitals $|0\rangle$ on atom C_0 and $|1\rangle$ on

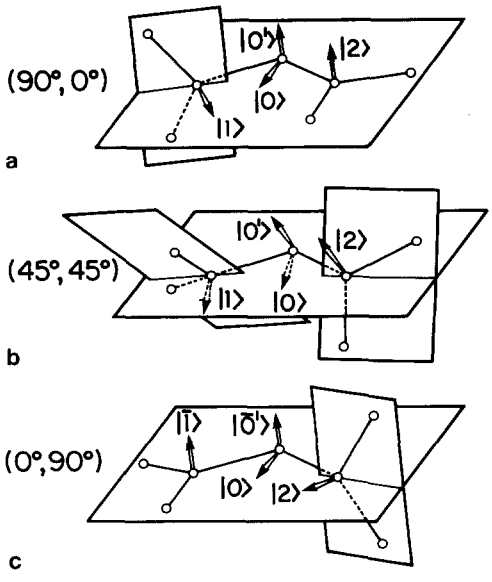

Fig. 3a–c. Positions of atoms and directions of quasi-atomic reactive FORS MOs in the valley $\delta_1 + \delta_2 = 90°$ for $\Phi = 100°$. Direction of reactive orbitals indicated by arrows representing unit vectors. *Dotted lines* imply objects behind or below the CCC or CHH planes. Numbers above **a**, **b**, **c** indicate (δ_1, δ_2). In **Fig. 3c**, the labels $|\bar{0}'\rangle, |\bar{1}\rangle$ indicate that these *orbitals* point in directions opposite to those of the *arrows*

atom C_1. Localization of the latter yields the perpendicular orbitals $|2\rangle$ on atom C_2 and $|0'\rangle$ on atom C_0 (see Fig. 1). The unit vectors of the directions in which these four quasi-atomic FORS MOs point are indicated in Fig. 3a. *Contours* of the two quasi-atomic FORS MOs of A'' symmetry are exhibited in Fig. 4a; they are drawn in the plane *perpendicular to the CCC plane* and containing the atoms C_0 and C_2. The bold contours depict orbital $|0'\rangle$, the weaker contours represent orbital $|2\rangle$. It is apparent that these two quasiatomic FORS MOs correspond to two p-orbitals on atoms C_0 and C_2 whose overlap is sufficient for the formation of a π-bond. Contours of the quasiatomic FORS MOs of A' symmetry are exhibited in Fig. 4b. They are drawn *in the CCC plane*, the bold contours corresponding to $|0\rangle$ and the lighter contours corresponding to $|1\rangle$. The overlap between these two orbitals is noticeably weaker so that they are in a less favorable position for π-bonding. (Note that the meaning of solid and dashed contours is different in Fig. 4a,b.)

($\delta_1 = \delta_2 = 45°$). The intermediate geometry $\delta_1 = \delta_2 = 45°$, which has C_2 symmetry is shown in Fig. 3b. Here the localization was performed simultaneously on all four reaction orbitals. The quasiatomic FORS MOs on the central atom are chosen as two equivalent hybrid-type orbitals rather than σ and π. Nonetheless, we still denote them as $|0\rangle$ and $|0'\rangle$. The directions of the quasi-atomic FORS MOs are again indicated by unit vectors in Fig. 3b. The geometry of Fig. 3b can be imagined to result from that of Fig. 3b as follows: The right-hand CH_2 group rotates in such a manner that orbital $|2\rangle$ tilts towards the viewer and the CH_2 group on the left rotates so that orbital $|1\rangle$ tilts its head below the CCC plane. Simultaneously, the orbitals $|0\rangle$ and $|0'\rangle$ on the central carbon rigidly rotate together in such a manner that $|0'\rangle$ tilts towards the viewer and $|0\rangle$ tilts below the CCC plane. A remarkable result is that *the two unit vectors marking the directions of* $|2\rangle$ *and* $|0'\rangle$ *as well as the bond vector* $\overrightarrow{C_0C_2}$ *almost lie in one plane.* In fact the plane spanned by $|2\rangle$ and $\overrightarrow{C_0C_2}$ forms an angle of 2° with the plane spanned by $|0'\rangle$ and $\overrightarrow{C_0C_2}$ We therefore choose the plane halfway in between

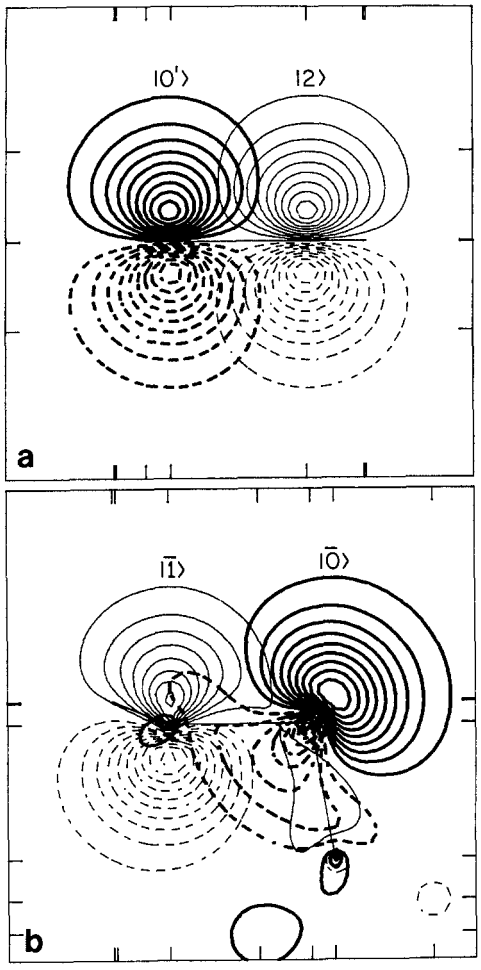

Fig. 4a,b. Quasi-atomic reactive FORS MOs for $\Phi = 100°$ and $(\delta_1, \delta_2) = (90°, 0°)$. **a** Drawing plane perpendicular to CCC plane; *solid lines* = positive; *dashed lines* = negative. **b** Drawing plane in CCC plane, *dashed lines* = positive, *solid lines* = negative

these two planes for drawing the contours of the quasi-atomic FORS MOs $|0'\rangle$ and $|2\rangle$. They are shown in Fig. 5a. The situation is entirely analogous for the orbitals $|1\rangle$ and $|0\rangle$. The contours for these orbitals are shown in Fig. 5b. It is apparent that both orbital pairs exhibit a sizable overlap so that bonding interactions can develop between the partners of each pair. As before, the orbitals $|0\rangle$ and $|0'\rangle$ are given by bold contours.

$(\delta_1, \delta_2) = (0°, 90°)$. The positions of the atoms for the geometry $(\delta_1 = 0°, \delta_2 = 90°)$ are shown in Fig. 3c. The directions of the quasi-atomic FORS MOs are again indicated by unit vectors. The geometry 3c can be imagined to result from that of Fig. 3b by continuing the rotations which led from 3a to 3b. Thereby orbitals $|2\rangle$ and $|0'\rangle$ should end up lying in the CCC plane whereas orbitals $|1\rangle$ and $|0'\rangle$ should end up perpendicular to the CCC plane pointing below that plane. In Fig. 3c, we have, however, exchanged the labeling for the orbitals $|0\rangle$, $|0'\rangle$ so that as was the case for $(\delta_1 = 90°, \delta_2 = 0°)$, $|0\rangle$ denotes again the in-plane orbital and $|0'\rangle$ denotes again the perpendicular orbital. Hence, $|0\rangle$ of Fig. 3b rotates into $|0'\rangle$ of Fig. 3c and $|0'\rangle$ of Fig. 3d rotates into $|0\rangle$ of Fig. 3c.

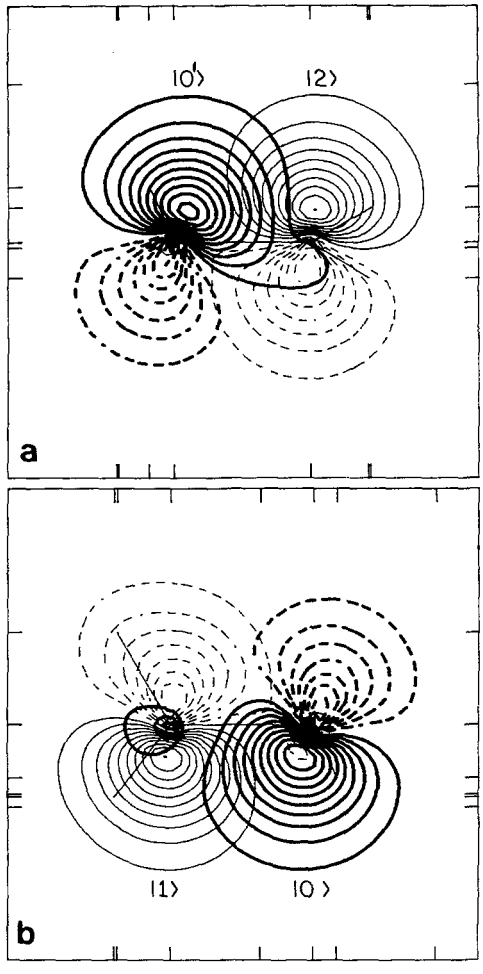

Fig. 5a,b. Quasi-atomic reactive FORS MOs for $\Phi = 100°$ and $(\delta_1, \delta_2) = (45°, 45°)$. For explanation of drawing planes see text. *Solid lines* = positive, *dashed lines* = negative

(Note also that the arrows drawn correspond to the orbitals $-|1\rangle$ and $-|0'\rangle$, pointing upward, and are therefore labeled as $|\bar{1}\rangle = -|1\rangle$ and $|\bar{0}'\rangle = -|0'\rangle$.) It is apparent that the roles of the orbitals $|1\rangle$ and $|2\rangle$ are now reversed in that the arrangement is favorable for a π-bond between $|1\rangle$ and $|0'\rangle$, perpendicular to the CCC plane, while a weaker π-bond will be formed between $|2\rangle$ and $|0\rangle$ in the CCC plane.

5.2. *Analysis for* $(\delta_1, \delta_2) = (90°, 0°)$ *and* $(\delta_1, \delta_2) = (0°, 90°)$

Population and bond order analysis. The density matrices in terms of these quasi-atomic orbitals are given in Table 11A and C. The occupation numbers of all four orbitals $|0\rangle$, $|0'\rangle$, $|1\rangle$, $|2\rangle$ are close to unity. In the case $(\delta_1, \delta_2) = (90°, 0°)$ of Table 11A, positive bond orders exist for the orbital pair $|0\rangle$, $|1\rangle$ and for the orbital pair $|0'\rangle$, $|2\rangle$. The fact that bonding can occur in both of these pairs accounts for almost an entire electron having been promoted from the σ orbital

Table 11. Occupation numbers and bond orders of quasi-atomic orbitals along the isoenergetic valley for $\Phi = 100°$

A. Density matrix coefficients p_{ij} for $(\delta_1, \delta_2) = (90°, 0°)$

	$\|0\rangle$	$\|0'\rangle$	$\|1\rangle$	$\|2\rangle$
$\|0\rangle$	1.06711	0	0.68621	0
$\|0'\rangle$	0	0.96612	0	0.84087
$\|1\rangle$	0.68621	0	0.93259	0
$\|2\rangle$	0	0.84087	0	1.03421

B. Density matrix coefficients p_{ij} for $(\delta_1, \delta_2) = (45°, 45°)$

	$\|0\rangle$	$\|0'\rangle$	$\|1\rangle$	$\|2\rangle$
$\|0\rangle$	1.02020	0.11118	0.74928	−0.03815
$\|0'\rangle$	0.11118	1.02020	−0.03815	0.74928
$\|1\rangle$	0.74928	−0.03815	0.97981	−0.07665
$\|2\rangle$	−0.03815	0.74928	−0.07665	0.97981

C. Density matrix coefficients p_{ij} for $(\delta_1, \delta_2) = (0°, 90°)$

	$\|0\rangle$	$\|0'\rangle$	$\|1\rangle$	$\|2\rangle$
$\|0\rangle$	1.06711	0	0	0.68621
$\|0'\rangle$	0	0.96612	0.84087	0
$\|1\rangle$	0	0.84087	1.03421	0
$\|2\rangle$	0.68621	0	0	0.93259

$|0\rangle$ to the π-orbital $|0'\rangle$ at the central carbon. It is, however, apparent that the electron attraction power of $|0\rangle$ is still larger than that of $|0'\rangle$ because, taking a unit occupation of all four orbitals as reference, a charge of 0.068 electrons has moved from $|1\rangle$ to $|0\rangle$ whereas a charge of 0.034 has moved in the opposite direction, viz. from $|0'\rangle$ to $|2\rangle$. In total, a charge in the amount of 0.034 electron has been transferred to the central carbon. The bond $|0\rangle - |1\rangle$ has a considerably weaker bond order than the bond $|0'\rangle - |2\rangle$, as we expected from the overlaps inferred from Fig. 4. The roles of the orbitals $|1\rangle$ and $|2\rangle$ are manifestly reversed in the density matrix for the geometry $(\delta_1, \delta_2) = (0°, 90°)$ shown in Fig. 3c.

The expansions of the *natural* FORS MOs in terms of the quasi-atomic FORS MOs are listed in Table 12A for $(\delta_1, \delta_2) = (90°, 0°)$ and illuminate the foregoing conclusions from a somewhat different angle. It is apparent that there exists one bonding MO $|01b\rangle$ between the quasi-atomic orbitals $|0\rangle$ and $|1\rangle$ (first column) and another bonding MO $|0'2b\rangle$ between the quasi-atomic orbitals $|0'\rangle$ and $|2\rangle$ (third column). To each of them there exists a correlating orbital (columns two and four) and each correlated bond embodies exactly two electrons. In agreement with the preceding charge transfer observation, the bond involving $|0\rangle$ is polarized towards C_0 whereas the bond involving $|0'\rangle$ is polarized away from C_0 towards C_2. Furthermore, the relative occupations of the bonding and antibonding orbitals imply that the in-plane bond involving $|0\rangle$ is weaker than the out-of-plane bond involving $|0'\rangle$. Table 12C shows the analogous results for $(\delta_1, \delta_2) = (0°, 90°)$ with the roles of $|1\rangle$ and $|2\rangle$ reversed.

The integrated and compacted representation in form of the population and bond order analysis, given in Tables 13A, 13C, 14A, 14C confirms these conclusions.

Table 12. Natural FORS MOs and chemically localized FORs MOs for $\Phi = 100°$

A. $\delta_1 = 90°$, $\delta_2 = 0°$				
	$\|01b\rangle$	$\|01c\rangle$	$\|0'2b\rangle$	$\|0'2c\rangle$
$\|0\rangle$	0.740793	−0.671733	0	0
$\|0'\rangle$	0	0	0.692656	0.721268
$\|1\rangle$	0.671733	0.740793	0	0
$\|2\rangle$	0	0	0.721268	−0.692656
N_n	1.689348	0.310352	1.841724	0.158606
Sum	1.99970		2.00033	
B. $\delta_1 = \delta_2 = 45°$, natural MOs				
	|A-bond⟩	|A-corr⟩	|B-bond⟩	|B-corr⟩
$\|0\rangle$	0.538153	−0.458684	−0.476127	0.522784
$\|0'\rangle$	0.538153	−0.458684	0.476127	−0.522784
$\|1\rangle$	0.458684	0.538153	−0.522784	−0.476127
$\|2\rangle$	0.458684	0.538153	0.522784	0.476127
N_n	1.737490	0.297050	1.773617	0.191863
Sum	2.03454		1.965480	
B′. $\delta_1 = \delta_2 = 45°$, chemically localized MOs				
	$\|01b\rangle$	$\|01c\rangle$	$\|0'2b\rangle$	$\|0'2c\rangle$
$\|0\rangle$	0.717204	−0.694003	0.043859	0.045326
$\|0'\rangle$	0.043859	0.045326	0.717204	−0.694003
$\|1\rangle$	0.694003	0.717204	−0.045326	0.043859
$\|2\rangle$	−0.045326	0.043859	0.694003	0.717204
N_n	1.755554	0.244457	1.755554	0.244457
Sum	2.000011		2.000011	
C. $\delta_1 = 0°$, $\delta_2 = 90°$				
	$\|02b\rangle$	$\|02c\rangle$	$\|0'1b\rangle$	$\|0'1c\rangle$
$\|0\rangle$	0.740793	−0.671733	0	0
$\|0'\rangle$	0	0	0.692656	0.721268
$\|1\rangle$	0	0	0.721268	−0.692656
$\|2\rangle$	0.671733	0.740793	0	0
N_n	1.689348	0.310352	1.841724	0.158606
Sum	1.99970		2.00033	

Configurational analysis. Table 15 lists the expansion coefficients of the FORS wavefunctions in terms of the configurations formed from quasi-atomic FORS MOs for the geometries under discussion. The first column applies to the case $(\delta_1, \delta_2) = (90°, 0°)$. Here, the normalized neutral base function without electron sharing is:

$$\Psi_B = 0.934|00'12T\rangle - 0.355|00'12S\rangle$$

and it has a weight of 65% in the total wavefunction. This expression for Ψ_B

Table 13. FORS population analysis for $\Phi = 100°$

A. (90°, 0°)		Natural FORS MOs					
		$\|01b\rangle$	$\|01c\rangle$	$\|0'2b\rangle$	$\|0'2c\rangle$	p_{ii}	Atoms
Quasi-	$\|0\rangle$	0.92707	0.14004	0	0	1.06711	2.03323
atomic	$\|0'\rangle$	0	0	0.88361	0.08251	0.96612	
FORS	$\|1\rangle$	0.76228	0.17031	0	0	0.93259	1.96680
MOs	$\|2\rangle$	0	0	0.95812	0.07609	1.03421	
	N_n	1.68935	0.31035	1.84172	0.15861		
	Sum	1.99970		2.00033		4	4

B. (45°, 45°)		Natural FORS MOs					
		$\|$A-bond$\rangle$	$\|$A-corr$\rangle$	$\|$B-bond$\rangle$	$\|$B-corr$\rangle$	p_{ii}	Atoms
Quasi-	$\|0\rangle$	0.50319	0.06250	0.40207	0.05244	1.02020	2.04040
atomic	$\|0'\rangle$	0.50319	0.06250	0.40207	0.05244	1.02020	
FORS	$\|1\rangle$	0.36555	0.08603	0.48474	0.04349	0.97981	1.95962
MOs	$\|2\rangle$	0.36555	0.08603	0.48474	0.04349	0.97981	
	N_n	1.73749	0.29705	1.77362	0.19186		
	Sum	2.03454		1.96548		4	4

B′. (45°, 45°)		Chemically localized FORS MOs							
		$\|01b\rangle$	$\|01c\rangle$	$\|0'2b\rangle$	$\|0'2c\rangle$	$\|b\rangle\|b'\rangle$	$\|c\rangle\|c'\rangle$	p_{ii}	Atoms
Quasi-	$\|0\rangle$	0.90303	0.11774	0.00338	0.00050	−0.00059	−0.00165	1.02241	2.04481
atomic	$\|0'\rangle$	0.00338	0.00050	0.90303	0.11774	−0.00059	−0.00165	1.02241	
FORS	$\|1\rangle$	0.84555	0.12574	0.00361	0.00047	0.00059	0.00165	0.97761	0.97761
MOs	$\|2\rangle$	0.00361	0.00047	0.84555	0.12574	0.00059	0.00165	0.97761	0.97761
	N_n	1.75555	0.24446	1.75555	0.24446	0	0		
	Sum	2.00001		2.00001				4	4

C. (0°, 90°)		Natural FORs MOs					
		$\|02b\rangle$	$\|02c\rangle$	$\|0'1b\rangle$	$\|0'1c\rangle$	p_{ii}	Atoms
Quasi-	$\|0\rangle$	0.92707	0.14004	0	0	1.06711	2.03323
atomic	$\|0'\rangle$	0	0	0.88361	0.08251	0.96612	
FORS	$\|1\rangle$	0	0	0.95812	0.07609	1.03421	1.96680
MOs	$\|2\rangle$	0.76228	0.17031	0	0	0.93259	
	N_n	1.68935	0.31035	1.84172	0.15861		
	Sum	1.99970		2.00033		4	4

shows that for a CCC opening angle of 100° the orbitals $|0\rangle$ and $|0'\rangle$ on the central carbon are energetically competitive.

As mentioned before, the predominance of the triplet-coupled term (T) over the singlet-coupled term (S) is presumably due to an approximate "local Hund's rule". As emphasized above, this base function yields no covalent bonding, in the present case no π-bonding between C_0 and C_1 or C_2. Such bonding is the result

Table 14. FORS bond order analysis for $\Phi = 100°$

A. (90°, 0°)		Natural FORS MOs				
		$\|01b\rangle$	$\|01c\rangle$	$\|0'2b\rangle$	$\|0'2c\rangle$	p_{ij}
Quasi-	(00′)	0	0	0	0	0
atomic	(01)	0.84065	−0.15444	0	0	0.68621
FORS	(02)	0	0	0	0	0
MO	(0′1)	0	0	0	0	0
pairs	(0′2)	0	0	0.92011	−0.07924	0.84087
	(12)	0	0	0	0	0

B. (45°, 45°)		Natural FORS MOs				
		|A-bond⟩	|A-corr⟩	|B-bond⟩	|B-corr⟩	p_{ij}
Quasi-	(00′)	0.50319	0.06250	−0.40207	−0.05244	0.11118
atomic	(01)	0.42889	−0.07332	0.44147	−0.04776	0.74928
FORS	(02)	0.42889	−0.07332	−0.44147	0.04776	−0.03814
MO	(0′1)	0.42889	−0.07332	−0.44147	0.04776	−0.03814
pairs	(0′2)	0.42889	−0.07332	0.44147	−0.04776	0.74928
	(12)	0.36555	0.08603	−0.48474	−0.04349	−0.07665

B′. (45°, 45°)		Chemically localized FORS MOs						
		$\|01b\rangle$	$\|01c\rangle$	$\|0'2b\rangle$	$\|0'2c\rangle$	$\|b\rangle\|b'\rangle$	$\|c\rangle\|c'\rangle$	p_{ij}
Quasi-	(00′)	0.05522	−0.00769	0.05522	−0.00769	−0.00960	0.02544	0.11090
atomic	(01)	0.87381	−0.12168	−0.00349	0.00049	0.00004	0.00011	0.74928
FORS	(02)	−0.05707	−0.00744	0.05344	0.00795	−0.00922	−0.02607	−0.03841
MO	(0′1)	0.05344	0.00795	−0.05707	−0.00744	−0.00922	−0.02607	−0.03841
pairs	(0′2)	−0.00349	0.00049	0.87381	−0.12168	0.00004	0.00011	0.74928
	(12)	−0.05522	0.00077	−0.05522	0.00769	−0.00900	0.02715	−0.08383

C. (0°, 90°)		Natural FORS MOs				
		$\|02b\rangle$	$\|02c\rangle$	$\|0'1b\rangle$	$\|0'1c\rangle$	p_{ij}
Quasi-	(00′)	0	0	0	0	0
atomic	(01)	0	0	0	0	0
FORS	(02)	0.84065	−0.15444	0	0	0.68621
MO	(0′1)	0	0	0.92011	−0.07924	0.84087
pairs	(0′2)	0	0	0	0	0
	(12)	0	0	0	0	0

of electron sharing resulting from the admixture of SAAPs providing for the appropriate electron jumps. Indeed, the SAAPs with the larger coefficients in the first column of Table 10 provide just the right terms:

For electron sharing between $|0'\rangle$ and $|2\rangle$:

$$R_{0'\to 2}\Psi_B = |2^2 01\rangle, \qquad R_{2\to 0'}\Psi_B = |0'^2 01\rangle,$$

and for electron sharing between $|0\rangle$ and $|1\rangle$:

$$R_{0\to 1}\Psi_B = |1^2 0'2\rangle, \qquad R_{1\to 0}\Psi_B = |0^2 0'2\rangle.$$

Table 15. Expansion coefficients of wavefunctions for three species in the isoenergetic valley for $\Phi = 100°$ in terms of configurations generated from quasi-atomic FORs MOs

SAAPS		90°, 0°	0°, 90°	45°, 45°
$C_0^0C_1^0C_2^0$:	$\|0^212\rangle$	−0.006216	0.006216	−0.073841
	$\|0'^212\rangle$	0.002979	−0.002979	−0.073841
	$\|00'12S\rangle$	−0.286549	−0.286549	−0.327543
	$\|00'12T\rangle$	0.752690	−0.752690	0.745284
$C_1^-C_2^+$:	$\|0^21^2\rangle$	−0.005821	0.152381	−0.010228
	$\|0'^21^2\rangle$	0.080091	−0.014741	0.105977
	$\|00'1^2\rangle$	−0.003956	−0.003289	0.021182
$C_1^+C_2^-$:	$\|0^22^2\rangle$	0.152381	−0.005821	0.105977
	$\|0'^22^2\rangle$	−0.014741	0.080091	−0.010228
	$\|00'2^2\rangle$	0.003289	0.003956	0.021182
$C_0^-C_1^+$:	$\|0^20'2\rangle$	0.279601	−0.004490	0.284827
	$\|0'^202\rangle$	−0.001292	0.299058	−0.008997
$C_0^+C_1^-$:	$\|021^2\rangle$	0.001785	0.332512	0.064810
	$\|0'21^2\rangle$	0.177873	0.002625	0.246137
$C_0^-C_2^+$:	$\|0^20'1\rangle$	0.004490	0.279601	−0.008997
	$\|0'^201\rangle$	0.299058	0.001292	0.284827
$C_0^+C_2^-$:	$\|012^2\rangle$	0.332512	−0.001785	0.246137
	$\|0'12^2\rangle$	−0.002625	0.177873	0.064810
$C_0^{2-}C_1^+C_2^+$:	$\|0^20'^2\rangle$	0.087876	0.087876	0.085405
$C_0^{2+}C_1^-C_2^-$:	$\|1^22^2\rangle$	0.061851	0.061851	0.059333

All other SAAPs contribute very little, except for $|0^22^2\rangle$ which can be understood as $R_{1\to 0}R_{0'\to 2}\Psi_B$. From the magnitude of the coefficients, it is also seen that, in accordance with our expectations, the interaction between $|0'\rangle$ and $|2\rangle$ is stronger than that between $|0\rangle$ and $|1\rangle$.

The case $(\delta_1, \delta_2) = (0°, 90°)$ is shown in the second column. It is apparent that this column of coefficients can be obtained from the first column by (i) changing the sign of $|0'\rangle$ and $|2\rangle$, (ii) interchanging $|1\rangle$ and $|2\rangle$, (iii) taking into account that $|00'21T\rangle = -|00'12T\rangle$.

5.3. *Analysis for* $\delta_1 = \delta_2 = 45°$

Population and bond order analysis. The density matrix for this case is listed in Table 11B. It is apparent that there exists perfect symmetry with respect to the end carbons. Orbital $|0\rangle$ has a bonding interaction with orbital $|1\rangle$ and a slight non-bonded repulsion with respect to orbital $|2\rangle$. Conversely, orbital $|0'\rangle$ has a bonding interaction with orbital $|2\rangle$ and a slight non-bonded repulsion with respect to orbital $|1\rangle$. An electronic charge in the amount of 0.020 electrons is transferred from orbital $|1\rangle$ to orbital $|0\rangle$ and equally from orbital $|2\rangle$ to orbital $|0'\rangle$, giving the central carbon an extra electronic charge of 0.040 quite similar to the total charge transfer of 0.034 to the central carbon for the cases $(\delta_1, \delta_2) = (90°, 0°)$ and $(0°, 90°)$. It is also noteworthy that the two identical

bond orders in this case, viz. 0.75, are approximately equal to the average of the two different bond orders for the previously considered case ($\delta_1 = 90°$, $\delta_2 = 0°$):

$$(0.8407 + 0.6854)/2 = (0.8407 \times 0.6854)^{1/2} \simeq 0.76.$$

This similarity fits in well with the near isoenergeticity of the three geometries.

Since the molecule has C_2 symmetry in this conformation, the natural orbitals have A and B symmetry. Their expansion in terms of the quasiatomic orbitals, displayed in Table 12C, shows that, because of the symmetry adaption, they mix up the two bonds. Greater clarity is therefore obtained by going over to the *chemically localized* FORS MOs discussed as the end of Sect. 2.2. In the present case, the separate localizations of the strongly and the weakly occupied natural orbitals |A-bond⟩ and |B-bond⟩ is readily accomplished by inspection, viz.:

$$|01b\rangle = \{|\text{A-bond}\rangle - |\text{B-bond}\rangle\}/\sqrt{2},$$
$$|01c\rangle = \{|\text{A-corr}\rangle - |\text{B-corr}\rangle\}/\sqrt{2},$$
$$|0'2b\rangle = \{|\text{A-bond}\rangle + |\text{B-bond}\rangle\}/\sqrt{2},$$
$$|0'2c\rangle = \{|\text{A-corr}\rangle + |\text{B-corr}\rangle\}/\sqrt{2}.$$

From their expansions in terms of the quasiatomic orbitals, listed in Table 12B′, it is apparent that the first two describe bonding and correlation between |0⟩ and |1⟩, whereas the last two do so between |0′⟩ and |2⟩. The density matrix between these orbitals, given by Table 16, shows that they are still near-natural. Tables 13B′ and 14B′ display the population and bond order analysis in terms of these chemically adapted orbitals. Since they are not exactly natural orbitals, small crossterms must be listed for them. These tables confirm our conclusions regarding populations and bonding.

Configurational analysis. These conclusions are also reflected in the expansion coefficients for the wavefunction which are listed in the last column of Table 15. In this case the neutral base function without electron sharing is:

$$\Psi_B = 0.915|00'12T\rangle - 0.402|00'12S\rangle$$

and it represents 66% of the wavefunction. It is readily seen that the remaining major contributors to this wavefunction are SAAPs which establish electron sharing between the orbitals |0⟩ and |2⟩ and between the orbitals |0′⟩ and |1⟩, namely:

$$R_{0\to 1}\Psi_B = |1^20'2\rangle, \qquad R_{1\to 0}\Psi_B = |0^20'2\rangle,$$
$$R_{0'\to 2}\Psi_B = |2^201\rangle, \qquad R_{2\to 0'}\Psi_B = |0'^201\rangle,$$

Table 16. Density matrix in terms of chemically adapted orbitals for $\Phi = 100°$ and $\delta_1 = \delta_2 = 45°$

	$\|01b\rangle$	$\|01c\rangle$	$\|0'2b\rangle$	$\|0'2c\rangle$
$\|01b\rangle$	1.75555	0	−0.01860	0
$\|01c\rangle$	0	0.24446	0	0.05259
$\|0'2b\rangle$	−0.01860	0	1.75555	0
$\|0'2c\rangle$	0	0.05259	0	0.24446

and to a lesser extent:

$$R_{0'\to 2}R_{1\to 0}\Psi_B = |0^2 2^2\rangle, \qquad R_{2\to 0'}R_{0\to 1}\Psi_B = |0'^2 1^2\rangle.$$

It is apparent that the CI expansions of all three columns are very similar.

In summary, we infer that the binding energy generated by each of the twisted π-bonds in the (45°, 45°) geometry is about the *average* of the binding energies of the two different π-bonds found for the (0°, 90°) and the (90°, 0°) geometries and that this accounts for the isoenergetic shelf which corresponds to the free synchronized CH_2 rotations.

6. Population and configuration analysis for the extended basis set calculations

The analyses in Sects 3–5 were based on the calculations reported in [1]. Since they were carried out with minimal basis sets, the question arises whether the interpretability in terms of atomic building blocks is a consequence of this restriction. In order to show that the atomic interpretability is in fact basis-set independent, we present in this section analogous analyses of calculations made with considerably higher accuracy. While we maintain the 20-dimensional FORS space spanned by four reactive orbitals, we expand the molecular orbitals in terms of an extended contracted basis with polarization functions, viz. the Dunning–Hay basis ($9s5p1d/3s2p1d$) for carbon and ($4s/2s$) for hydrogen. The details of these calculations and of the consequences for the energy surface will be discussed in the subsequent paper [2]. Here we report the results of the analyses for the reactant cyclopropyplidene, the product allene, the ring-opening transition state and the allene isomerization transition state.

6.1. Quasi-atomic character of localized FORS MOs

The first question is whether it is possible to localize the four FORS molecular orbitals, obtained from the extended basis set calculations, sufficiently strongly so that they still have quasi-atomic character. Rather than drawing more contour plots of localized molecular orbitals, we examine here a more quantitative measure of their atomic character, namely: the projection of each of these orbitals on the basis of the optimal five *free-atom* orbitals $1s$, $2s$, $2px$, $2py$, $2pz$ of the atom on which the quasiatomic MO is allegedly concentrated. If the orthonormal orbitals of that free atom are denoted by $\chi_1, \chi_2, \chi_3, \chi_4, \chi_5$, then the projection of a quasiatomic molecular orbital ϕ is given by:

$$\text{proj}(\phi) = \left\{ \sum_{j=1}^{5} \langle \chi_j / \phi \rangle^2 \right\}^{1/2}.$$

The optimal free-atom orbitals of the carbon atom were determined by a two-configuration MCSCF calculation of the ${}^3P(m_l = 0, m_s = 1)$ ground-state wavefunction:

$$c_1 A\{1s^2 2s^2 2px 2py\} + c_2 A\{1s^2 2pz^2 2px 2py\}$$

in the same contracted basis of the carbon atom which formed part of the basis for the molecular calculations (i.e., $9s5p1d/3s2p1d$).

Table 17 lists the projections of each of the four quasi-atomic molecular orbitals on the respective carbon free-atom basis at the four critical points of the

Table 17. Projection of quasi-atomic FORS MOs onto their respective free-atom bases (extended plus polarization basis calculation)

Critical	$\|0\rangle$ on C_0	$\|0'\rangle$ on C_0	$\|1\rangle$ on C_1	$\|2\rangle$ on C_2
Cyclopropylidene	0.9876	0.9590	0.9466	0.9466
Ring-opening transition state	0.9777	0.9585	0.9666	0.9666
Allene	0.9534	0.9634	0.9855	0.9855
Allene isomerization TS	0.9327	0.9780	0.9850	0.9850

energy surface. All of them lie between 0.93 and 0.99. It is clearly possible to find a transformation among the FORS molecular orbital such that all resulting molecular orbitals have strong quasiatomic character. In view of this result, it stands to reason that maximizing these projections, as described in Sect. 2.4, would yield very similar orbitals.

It may be noted that the quasi-atomic molecular orbitals are mutually

Table 18. Population-bond order matrices for extended-plus-polarization basis calculations

Cyclopropylidene (compare Table 1A)

	$\|0\rangle$	$\|0'\rangle$	$\|1\rangle$	$\|2\rangle$
$\|0\rangle$	1.92959	0	−0.00311	−0.00311
$\|0'\rangle$	0	0.07041	0	0.97649
$\|1\rangle$	−0.00311	0	1.00001	0.97649
$\|2\rangle$	−0.00311	0	0.97649	1.00001

Ring-opening transition state (compare Table 1B)

	$\|0\rangle$	$\|0'\rangle$	$\|1\rangle$	$\|2\rangle$
$\|0\rangle$	1.96027	0	−0.00334	−0.00334
$\|0'\rangle$	0	0.26250	0.42708	0.42708
$\|1\rangle$	−0.00334	0.42708	0.88862	0.80832
$\|2\rangle$	−0.00334	0.42708	0.80832	0.88862

Allene (compare Table 6A)

	$\|0\rangle$	$\|0'\rangle$	$\|1\rangle$	$\|2\rangle$
$\|0\rangle$	0.95372	0	0.91900	0
$\|0'\rangle$	0	0.95372	0	0.91900
$\|1\rangle$	0.91900	0	1.04628	0
$\|2\rangle$	0	0.91900	0	1.04628

Allene isomerization transition state (compare Table 6B)

	$\|0\rangle$	$\|0'\rangle$	$\|1\rangle$	$\|2\rangle$
$\|0\rangle$	1.00000	0	0	0
$\|0'\rangle$	0	0.98321	0.62642	0.62642
$\|1\rangle$	0	0.62642	1.00840	0.00840
$\|2\rangle$	0	0.62642	0.00840	1.00840

orthogonal. It is obviously possible to determine *non-orthogonal* molecular orbitals with even greater atomic projections while still spanning the same space of FORS MOs.

6.2. *Population analysis*

The population analysis is entirely determined by the population bond-order matrices between the quasi-atomic orbitals characterized by the projections of Table 17. These density matrices are listed in Table 18. They should be compared to the analogous matrices listed in Tables 1 and 6, as indicated on Table 18. It

Table 19. Natural orbitals and occupation numbers for extended plus polarization basis calculations

Cyclopropylidene (compare Table 2A)				
	$\|lp\rangle$	$\|lpc\rangle$	$\|12b\rangle$	$\|12c\rangle$
$\|0\rangle$	0.99572	0	−0.09245	0
$\|0'\rangle$	0	1	0	0
$\|1\rangle$	0.06537	0	0.70408	0.70711
$\|2\rangle$	0.06537	0	0.70408	−0.70711
N_n	1.92918	0.07041	1.97690	0.02352
Sum	1.99959		2.00042	

Ring-opening transition state (compare Table 2B)				
	$\|lp\rangle$	$\|lpc\rangle$	$\|10'2b\rangle$	$\|10'2c\rangle$
$\|0\rangle$	0.99480	−0.00084	0.10182	0
$\|0'\rangle$	0.03412	0.93939	0.34115	0
$\|1\rangle$	−0.06784	−0.24243	0.66078	0.70711
$\|2\rangle$	−0.06784	−0.24243	0.66078	−0.70711
N_n	1.96073	0.04206	1.91692	0.08030
Sum	2.00279		1.99721	

Allene (compare to Table 7A)				
	$\|01b\rangle$	$\|01c\rangle$	$\|0'2b\rangle$	$\|0'2c\rangle$
$\|0\rangle$	0.68910	0.72467	0	0
$\|0'\rangle$	0	0	0.68910	0.72467
$\|1\rangle$	0.72467	−0.68910	0	0
$\|2\rangle$	0	0	0.72467	−0.68910
N_n	1.92026	0.07984	1.92016	0.07984
Sum	2.00000		2.00000	

Allene isomerization transition state (compare to Table 7B)				
	$\|lp\rangle$	$\|12n\rangle$	$\|10'2b\rangle$	$\|10'2c\rangle$
$\|0\rangle$	1	0	0	0
$\|0'\rangle$	0	0	0.70037	0.71378
$\|1\rangle$	0	0.70711	0.50472	−0.49524
$\|2\rangle$	0	−0.70711	0.50472	−0.49524
N_n	1.00000	1.00000	1.88605	0.11395
Sum	2.00000		2.00000	

Table 20. Expansion coefficients for FORS wavefunctions determined with the extended plus polarization basis in terms of configurations generated from quasi-atomic FORS MOs

SAAPs[a]	Cyclopropylidene reactant[b]	Ring-opening transition state[b]	Allene product[c]	Allene isomerization transition state[c]
$\|0^2 12\rangle$	0.765408	0.740695	0	0
$\|0'^2 12\rangle$	−0.145899	−0.120286	0	0
$\|00'12S\rangle$	0	0.006387	0.691221	0.698631
$\|00'12T\rangle$	0	0	0.038554	−0.403355
$\|0^2 1^2\rangle$	0.435218	0.327408	−0.005663	0
$\|0'^2 1^2\rangle$	−0.083085	−0.050827	0.163483	0
$\|00'1^2\rangle$	0	0.004634	0	0.114835
$\|0^2 2^2\rangle$	0.435218	0.327408	0.163483	0
$\|0'^2 2^2\rangle$	−0.083085	−0.050827	−0.005663	0
$\|00'2^2\rangle$	0	0.004634	0	−0.114835
$\|0^2 0'2\rangle$	0	0.324581	0.299135	0
$\|0'^2 02\rangle$	0.007356	−0.002941	0	0.276610
$\|021^2\rangle$	0.007614	0.012779	0	0.291393
$\|0'21^2\rangle$	0	0.002704	0.350872	0
$\|0^2 0'1\rangle$	0	0.324581	0	0
$\|0'^2 01\rangle$	0.007356	−0.002941	0.299135	−0.276610
$\|012^2\rangle$	0.007614	0.012779	0.350872	−0.291393
$\|0'12^2\rangle$	0	0.002704	0	0
$\|0^2 0'^2\rangle$	−0.001141	0.078708	0.121189	0
$\|1^2 2^2\rangle$	−0.001441	−0.000890	0.165338	0

[a] SAAP = spin adapted antisymmetrized product
[b] Compare to Table 5
[c] Compare to Table 10

is evident that the results for the accurate calculations are very similar to those for the minimal-basis-set calculations. The quantitative differences are extremely small.

Alternatively, one can compare the spectral representations of these matrices, i.e., the natural orbitals and their occupation numbers. They are listed in Table 19 which corresponds to Tables 2 and 7. This comparison reconfirms the conclusion that the analyses of the minimal-basis-set calculations and of the more accurate calculations lead to essentially identical results.

6.3. Configurational analysis

The expansions of the FORS wavefunctions in terms of the configurations generated by the quasi-atomic FORS MOs are listed in Table 20. The analogous expansions for the minimal basis set calculations were given in Tables 5 and 10. As expected (in view of the population analysis), the simpler and the more accurate calculations also agree closely in the CI coefficients of the wavefunctions, so that all inferences reached in the earlier sections regarding the interpretation of the wavefunctions and the energy changes remain valid.

The quantitative results of Tables 17 to 20 show that the analysis in terms of the "configuration-generating" quasi-atomic orbitals is independent of the "quantitative working" orbital basis set. We feel therefore justified to conclude that, in fact, it is independent of how the orbitals are expressed.

7. Conclusions

FORS wavefunctions are unambiguously defined and yield *molecule-intrinsic* orbitals. Arbitrary non-singular transformations are permissible among such FORS MOs and this freedom can be used for localization. The maximally localized FORS MOs are intrinsic molecular orbitals which, typically, have the character of slightly deformed free-atom SCF or MCSCF orbitals. They are basis-set-independent "*quasi-atomic MOs*".

For the discussed reactions it has been found that:

(i) the quasi-atomic FORS MOs form an effective basis for rigorously achieving the objective of Mulliken's population analysis of the electron density;

(ii) the expansion coefficients of the wavefunction in terms of configurations generated from the quasi-atomic FORS MOs can be related to chemical bonding;

(iii) energy changes along paths on the potential energy surface can be elucidated through analyses in terms of the quasi-atomic FORS MOs;

(iv) the conclusions obtained by such analyses are basis-set independent.

The results also suggest that the analyses of minimal-basis-set calculations are very similar to those of the corresponding extended-basis-set calculations. The essential difference between the two approximations is the *difference in magnitude of the projections of the quasi-atomic FORS MOs on the space of the free-atom MCSCF orbitals*. These projections are large (above 90% in our case) for both types of calculations but the projections of the *intrinsic* quasi-atomic FORS MOs (which are better approximated by the extended-basis calculations) are somewhat smaller than those of the minimal-basis calculations. While these orbital adjustments of the intrinsic quasi-atomic MOs are essential for insuring chemical usefulness of the predicted energy changes, they do not significantly diminish the quasi-atomic character of the orbitals.

It can be concluded that accurate molecular wavefunctions can often be expressed as superpositions of configurations generated from orthogonal molecular orbitals which differ only by small deformations from MCSCF orbitals of free atoms. "Sometimes a little bit goes a long way" was R.S. Mulliken's interpretation of the fact that small orbital modifications often have marked effects on energy differences of chemical importance [8].

References

1. Valtazanos P, Elbert ST, Xantheas S, Ruedenberg K (1991) Theor Chim Acta 78:287 (Paper 1)
2. Xantheas S, Elbert ST, Rudenberg K (1991) Theor Chim Acta 78:365 (Paper 3)
3a. The FORS model was first formulated by Rudenberg K, Sundberg KR (1976) in: Calais JL, Goscinski O, Linderberg J, Ohrn Y (eds) Quantum science, Plenum Press, New York, p 505. Applications including wavefunctions up to 1700 configurations were made by Ruedenberg,

Sundberg, Cheung, Gilbert and Elbert and reported by Ruedenberg K (1978) in: Proceedings of the 1978 NRCC Workshop on the Post Hartree–Fock and Configuration Interaction Methods, Report LBL 8233, UC4, CONF 780833, Lawrence Berkeley Laboratory, Univ of California, p 46. See also Gilbert Dombek M (1977) Ph.D. thesis, Iowa State University. Further references are given in Ref. [3b]. The FORs model was conceived as the full MCSCF optimized wavefunction in the full valence space or a relevant subspace thereof. Subsequently, Roos, Siegbahn, and co-workers have generalized the approach to include very large full configuration spaces (CASSCF method) on the basis of a very effective implementations using direct CI and GUGA methods

3b. Ruedenberg K, Schmidt MW, Gilbert MM, Elbert SS (1982) Chemical Physics 71:41; (1982) 71:51; (1982) 71:65

4. Lowdin PO (1955) Phys Rev 97:1474

5. a. Mulliken RS (1955) J Chem Phys 23:1833, 1841, 2338, 2343
   b. A review is given in Sect II.E. of Mulliken RS, Ermler WC (1977) Diatomic molecules, Academic Press, New York

6. Edmiston C, Ruedenberg K (1963) Rev Mod Phys 35:457; England W, Salmon LS, Ruedenberg K (1971) Topics in Current Chemistry 23:31 and references therein

7. Ruedenberg K et al. (to be published)

8. Mulliken RS (personal communication)